A Novel Approach to Propagate MHz EM Signals and Map Reservoir Saturation Hundreds of Meters Away from the Wellbore

Jesus M. Felix Servin, Dr. Max Deffenbaugh, Robert W. Adams, and Dr. Val Riachentsev

Abstract /

This study describes a novel approach to propagate high frequency (MHz) electromagnetic (EM) signals through the subsurface. Our technique relies on the presence of subsurface transmission lines, in the form of highly resistive evaporite seals bounded by hydrocarbon reservoirs, to achieve greatly increased EM propagation. As the signal propagates through the seal, variations in the fluid saturation of the bounding reservoirs modulates the signal amplitude and velocity, paving the way for improved EM surveys for reservoir characterization.

The concept, known as proximity sensing, has been previously demonstrated via numerical simulations and laboratory experiments. In this work, we present quantitative 3D numerical simulations in the frequency domain to estimate the maximum depth of investigation (DOI) under multiple reservoir saturation scenarios. The models consist of three layers, representing an evaporite seal bounded by hydrocarbon reservoirs, two cased wellbores and two dipole antennas, representing the transmitter and receiver, respectively. Multiple parameters, including antenna location, wellbore fluid properties, reservoir saturation as well as seal conductivity, were evaluated to quantify their impact on the maximum DOI.

The results show that EM signals can propagate for over half a kilometer if the resistivity of the seal is high at frequencies — in the tens of Mhz. The relationship of the bounding reservoirs' conductivity and signal attenuation is clearly shown, and supports the possibility of using this method to map reservoir saturation. The evaporite and bounding reservoir's conductivities together with antenna depth were found to have the most significant effect on the maximum DOI. It was found that the wellbore fluid conductivity has a negligible effect on the DOI. Overall, the more conductive the bounding reservoirs are, the more efficient they are at containing the signal within the channel. Subsequently, more conductive reservoirs translate into higher signal attenuation before it enters the channel. Therefore, there is a tradeoff between reservoir conductivity and the maximum DOI.

The results presented confirm the viability of proximity sensing to propagate high frequency EM signals for hundreds of meters in the presence of conductive media and potentially provide valuable reservoir saturation information. This study provides additional insight as to the viability and ideal configuration for field testing and paves the way for a new research direction in EM surveys.

Introduction

Obtaining accurate reservoir saturation information at the interwell level is a long-standing challenge that would pave the way for improved reservoir management strategies. At present, logs can provide high resolution information, but it comes at the cost of the depth of investigation (DOI). Typical logging tools are limited to at most tens of meters into the formation. The most common methods to monitor reservoir saturation at the field scale include seismic and electromagnetic (EM) surveys. 4D seismic has been successfully applied, mostly in clastic reservoirs to monitor fluid movement[1-4], but it has shown mixed results when applied in carbonate reservoirs due to the fact that acoustic velocities of carbonates are relatively insensitive to changes of pressure and saturation[5, 6].

EM surveys, including crosswell EM[7], surface-to-borehole EM[8], and borehole-to-surface induced polarization[9-11], have recently been tested in carbonate reservoirs and show promising results. And while these approaches enable penetration in the kilometer range and have the potential to provide actionable information, their resolution is relatively low due to the use of low frequencies — typically between 1 Hz to 100 Hz. Therefore, alternative and complementary approaches with higher intrinsic resolution are desired.

Proximity sensing is a potential new approach to address the challenge of long range EM propagation in the reservoir, in the presence of conductive media. The proposed method relies on the use of naturally occurring waveguides in the form of a layer of sealing evaporite — such as anhydrite — bounded by conductive reservoirs. The hypothesis is that EM pulses traveling through a relatively nonconductive layer — such as evaporite seals — bounded by conductive layers — such as hydrocarbon reservoirs — will propagate with reduced attenuation and

the pulse's traveltime and attenuation will depend on the EM properties of the layers above and below. In other words, the resistive layer acts as a low-loss channel that enables the propagation of the EM signals far beyond typical ranges for the same signal traveling through the reservoir. At the same time, the speed of propagation and signal amplitude, when measured using multiple pairs of wells, can be inverted to provide a velocity map that can be interpreted into reservoir oil and water saturation.

The concept has been so far demonstrated through qualitative 2D and 3D numerical simulations[12-14] as well as laboratory experiments[15]. And while the sensitivity of the method to changes in saturation of the bounding fluids has been shown, the propagation range and the parameters controlling it had not been studied up until now. This study strives to estimate the propagation range under multiple reservoir saturation conditions as well as to determine which parameters should be considered toward the development and field testing of this approach.

Maximum Transmission Loss (MTL)

The applicability of proximity sensing to map reservoir saturation significantly depends on how far the signal can propagate before it is too weak to be detected for a desired traveltime measurement accuracy. To evaluate the propagation range, we have defined the maximum transmission loss (MTL) before the signal it is too weak to be detected as follows:

$$TL(dB) = P_{xmit}(dB) - P_{noise}(dB) + 10 * \log_{10} T + 16 + 20 * \log_{10} f + 20 * \log_{10} std[t] \quad (1)$$

where TL is the transmission loss in dB, P_{xmit} is the transmitter power in dB, T is the averaging time in seconds, f is the frequency in Hz, and $std[t]$ is the standard deviation of the measured traveltime.

A system capable of providing 200 W (400 V and 500 mA) was considered for this study. It was estimated that after cable and circuit losses, half of this power (100 W) will be delivered to the transmitter (Tx) antenna.

It was also assumed that the limiting source of noise is the circuit noise in the antenna amplifier is due to the Johnson noise, the voltage noise in the amplifier, and the current noise through the antenna impedance.

Together, the estimated noise level is no lower than 1×10^{-19} W/Hz. Assuming 10,000 seconds of averaging time, the MTL for 10 nanoseconds of accuracy in traveltime measurements at operating frequencies ranging from 6.7 MHz to 53.7 MHz was estimated to be between 243 dB and 261 dB, Table 1.

It is worth noting that higher frequencies result in greater MTL. This is expected because for a fixed averaging time, higher frequencies translate into a greater number of waveforms being averaged, and therefore, a higher signal level. The difference between the highest and lowest frequency considered in this study is no more than 18 dB.

Numerical Simulations

Quantitative 3D numerical simulations were performed in the frequency domain to estimate the maximum DOI for multiple configurations and reservoir properties. The maximum DOI was defined as the point where the signal attenuation reached the MTL defined in the previous section. The simulations were performed using a commercially available multiphysics software running on a cluster node with 20 processing cores and 196 GB of RAM.

The numerical models consisted of three layers, representing a hydrocarbon reservoir A (A), resistive seal (RS) and hydrocarbon reservoir B (B), respectively. The models included two fluid filled cased wellbores. The Tx and receiver (Rx) were located inside the wellbores in a crosswell configuration, Fig. 1.

Both the Tx and Rx were simulated as half-wave dipole antennas composed of two hollow arms separated by a gap, Fig. 2. The Tx power source was not explicitly modeled. Instead, the lumped port condition was used to apply a uniform voltage across the faces of the dipole

Table 1 *MTL as a function of frequency.*

Wavelength (m)	Frequency (MHz)	MTL (dB)
2.5	53.7	261
5	26.8	255
7.5	17.9	251
10	13.4	249
12.5	10.7	247
15	8.9	245
17.5	7.7	244
20	6.7	243

Fig. 1 *Schematic of the model showing three layers and two wellbores. The Tx was placed inside the wellbore at the center of the model; the Rx was placed inside the wellbore close to the right edge of the model.*

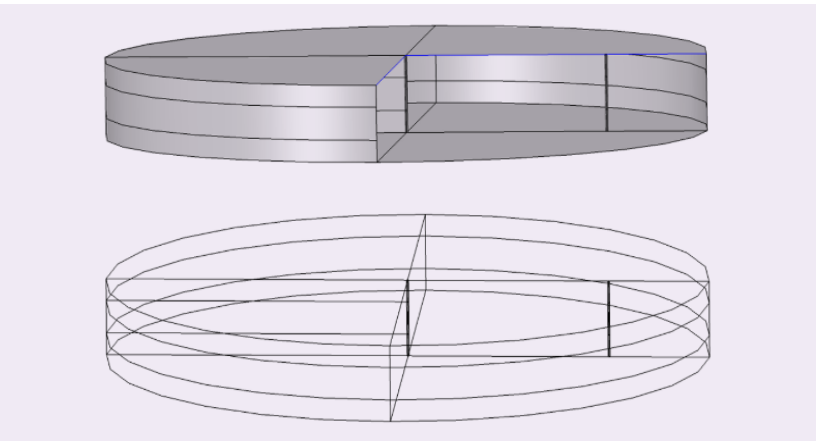

Fig. 2 *Schematic of the Tx and Rx. Each arm has the length of one-quarter of a wavelength. The highlighted section represents the gap between the arms.*

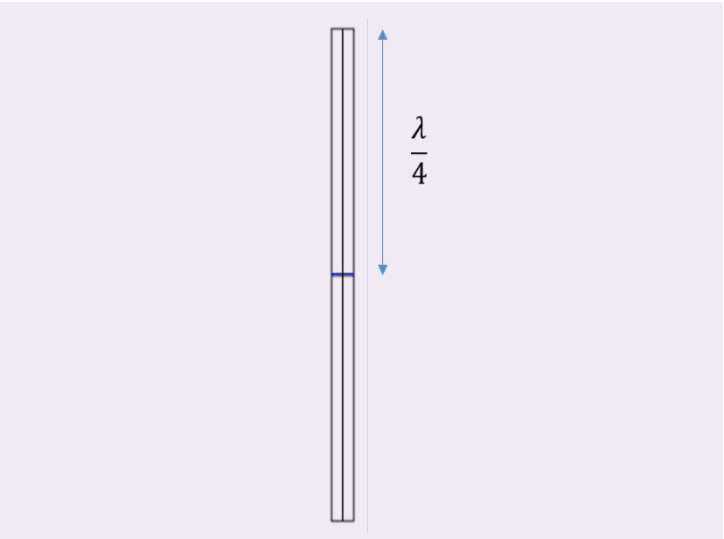

Fig. 3 *For all simulations, the well casing runs across reservoir A and the RS and stops at the interface of the RS and the reservoir B.*

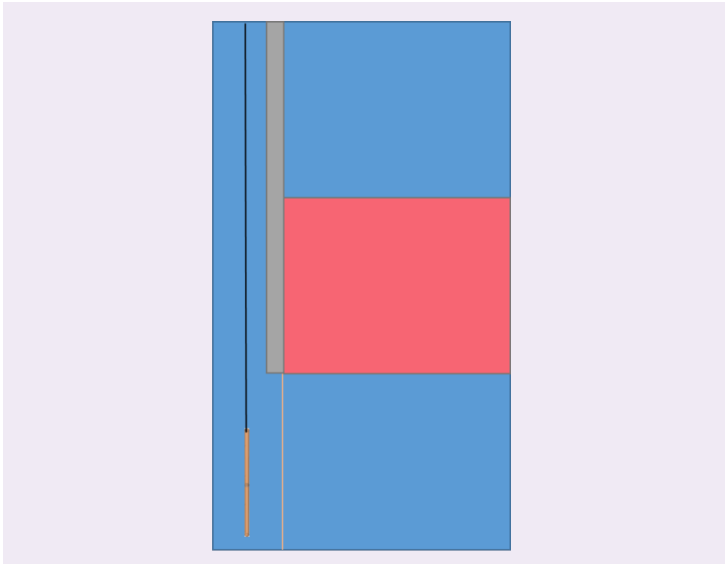

arms. For all scenarios the voltage applied across the arms of the Tx was 1 V. The voltage between the arms of the Rx was estimated as the voltage induced between the arms, due to the currents generated along the dipole arms as a result of the electric field.

Signal attenuation in *dB* for a given distance between the Tx and Rx was calculated as follows:

$$Att(dB) = 20\ log\left(\frac{V_{Rx}}{V_{Tx}}\right) \quad (2)$$

where *Att* is the signal attenuation in *dB*, V_{Tx} is the voltage applied between the arms of the Tx, and V_{Rx} is the voltage measured between the arms of the Rx.

Each layer was assigned three EM properties: electric conductivity (σ), relative electric permittivity (ε), and relative magnetic permeability (*m*), to represent an evaporite seal or a hydrocarbon reservoir with a determined fluid saturation, Table 2.

For all simulations presented in this study, the well casing runs across reservoir A and the RS, and stops at the interface of the RS and reservoir B, Fig. 3. Three saturation conditions were simulated: Reservoirs A and B were brine saturated, reservoir A was brine saturated, reservoir B 50% oil and 50% brine saturated, and reservoir A was brine saturated and reservoir B was oil saturated. The corresponding EM properties are summarized in Table 2.

In the following sections a sensitivity analysis is performed to determine which parameters have the greatest impact on the maximum DOI under different saturation conditions.

Saturation Scenarios

Based on the fluid saturation of the bounding reservoirs, three scenarios were simulated:

1. **Scenario 1a:** Hydrocarbon reservoirs A and B were brine saturated.
2. **Scenario 1b:** Hydrocarbon reservoir A was brine saturated, hydrocarbon reservoir B was 50% oil saturated, and 50% brine saturated.
3. **Scenario 1c:** Hydrocarbon reservoir A was brine saturated, hydrocarbon reservoir B was oil saturated.

After setting up the model, numerical optimization was performed to reduce the simulation domain, and therefore, the run time for each scenario. It was found that for distances between the Tx and Rx of 100 m or more,

Table 2 *Summary of the three EM properties representing each layer of a hydrocarbon reservoir with a determined fluid saturation.*

Property	Brine Saturated	50% Oil, 50% Brine	Oil Saturated	Evaporite Seal
ϵ_r	14	9.072944	6.233579	5
μ_r	1	1	1	1
$\sigma[\frac{S}{m}]$	0.4	0.12377	0.018031	0.0001

Fig. 4 *Progressive reduction of the sector angle for optimization purposes.*

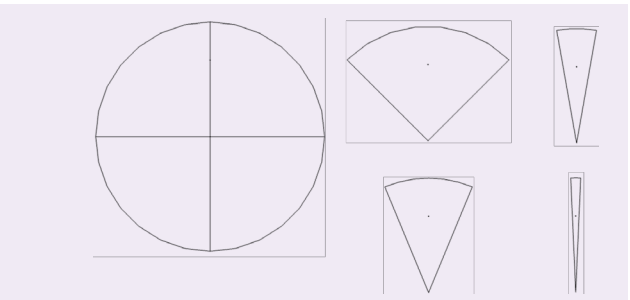

a 5° sector angle results in a solution almost identical to that of the entire domain. Therefore, a sector angle of 5° was used for all simulations presented, Fig. 4.

The thickness of the evaporite seal was assumed to be 10 m while each reservoir was assumed to be 90 m thick. Given the conductivity of the reservoirs, it was determined that the EM wave would not penetrate more than a few meters into the reservoirs. Therefore, the thickness of the bounding reservoirs was reduced to 2 m each to optimize the run time. This thickness was chosen because the results obtained were practically identical to the solutions using thicker reservoirs (data not shown).

Given that the hydrocarbon reservoirs, even if oil saturated, are much more conductive than the RS, the distance of the Tx and Rx to the interface should have a significant effect on attenuation. To evaluate the effect, simulations with different antenna depth were performed. For the purpose of this study, antenna depth was defined as the distance by which the center of the antenna was lowered from the center of the seal layer. Therefore, an antenna depth of 5 m means the center of the antenna is right at the RS and reservoir B interface. Similarly, an antenna depth of 6.5 m means the center of the antennas are 6.5 m below the center of the RS layer. In addition to varying antenna depth, the wavelength was also varied to evaluate the effect of frequency.

The results suggest that attenuation increases with increasing antenna depth and decreasing λ (increasing frequency), Fig. 5. While these results may suggest that using longer wavelengths is preferable, it must be noted that when using dipole antennas, the physical dimensions of the antenna are directly related to the frequency, and therefore wavelength. Subsequently, using lower frequencies, and therefore longer wavelengths, would mean that the center of the antennas would have to be further away from the RS reservoir B interface. Therefore, there is a tradeoff between low frequencies attenuating less, but resulting in the antennas being positioned further away from the interface, thereby resulting in greater overall attenuation.

To investigate the effect of antenna position alone, the operating frequency was chosen such that the equivalent λ inside the RS layer was 10 m, and the antenna depth was changed for a given Tx-Rx distance. The results confirm that antenna depth has a critical effect on signal attenuation. For a Tx-Rx distance of 100 m, lowering the antennas by an additional 0.7 m (from 5.8 m to 6.5 m) can result in up to a 50% increase in attenuation, Fig. 6. This means that accurate positioning of the tools in real life applications will be very important.

From the simulation results it can be concluded that

Fig. 5 *Attenuation as a function of wavelength for different antenna depths for scenario 1a (top), 1b (middle) and 1c (bottom). Slight changes in antenna depth (0.5 m) can result in significant increases in attenuation (44 dB). Both the wavelength and the antenna depth have a significant effect on attenuation.*

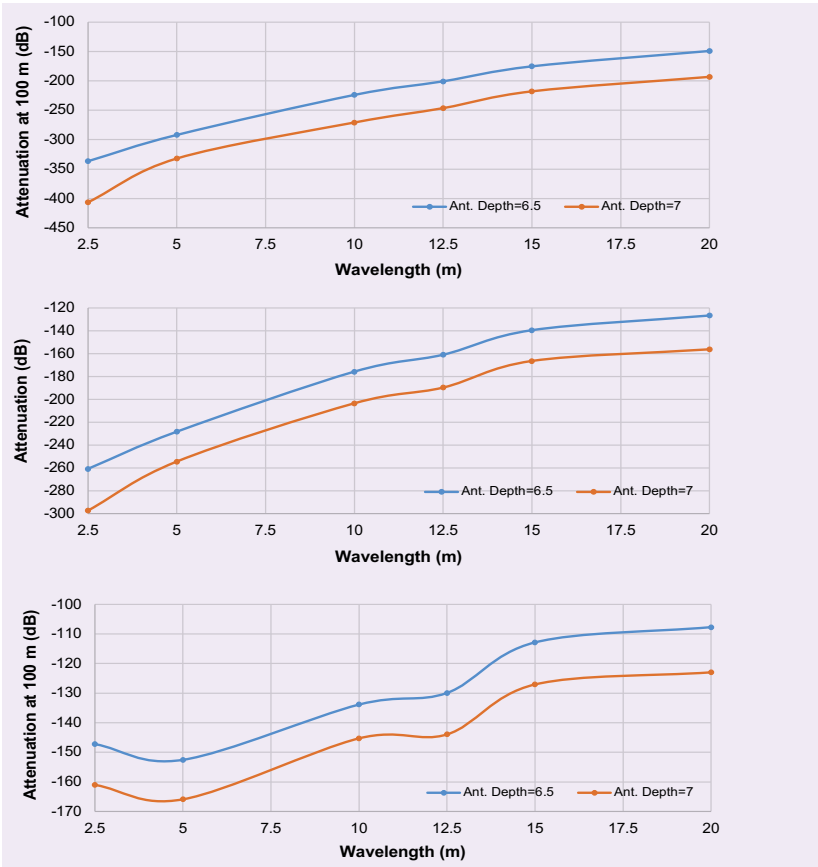

Fig. 6 *Attenuation as a function of depth for a Tx-Rx distance of 100 m for scenario 1a (bottom), 1b (middle) and 1c (top). Small changes in antenna depth result in significant changes in attenuation.*

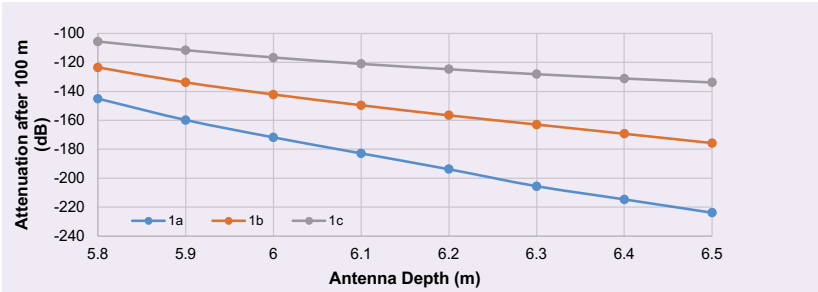

Fig. 7 *Attenuation as a function of distance for different RS conductivities for scenario 1a (top), 1b (middle) and 1c (bottom). Increasing the RS conductivity by one order of magnitude reduces five times the DOI.*

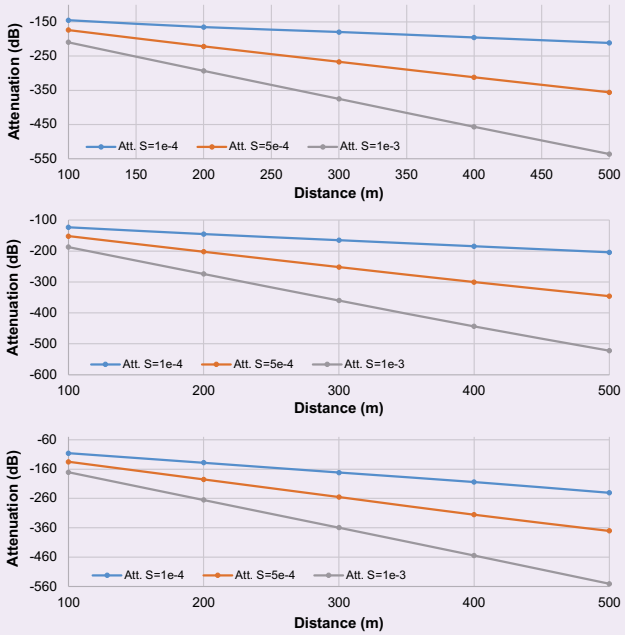

Fig. 8 *Attenuation as a function of distance for different wellbore fluid conductivity. Increasing the conductivity two orders of magnitude increases attenuation by 2 dB to 3 dB only.*

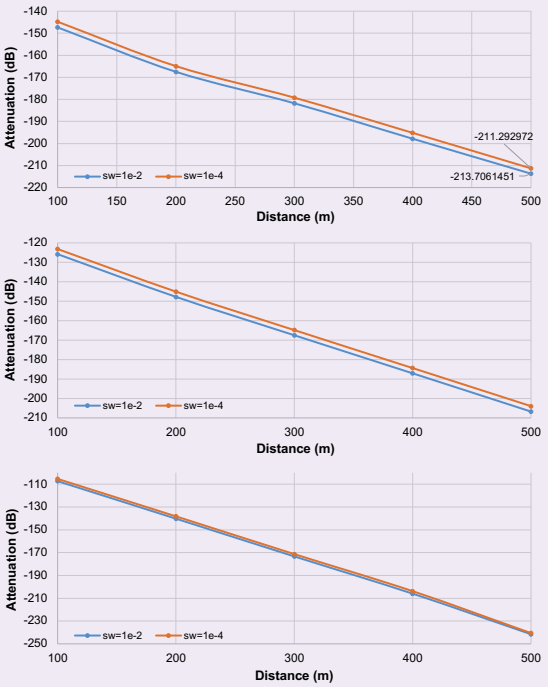

even when lower frequencies may appear as a better option at first, if the survey is to be carried out using dipole antennas, higher frequencies may result in reduced attenuation. On the other hand, the frequency should not be too high that it results in λ much smaller than the thickness of the RS, otherwise the proximity sensing approach will not work. For the following simulations, an operating frequency with an equivalent λ of 10 m in the RS — same as the RS thickness — was used.

The conductivity of evaporite seals can range across one to two orders of magnitude. To investigate the effect of such changes in the signal attenuation, three different values were simulated (1×10^{-4}, 5×10^{-4}, and 1×10^{-3} S/m). The results suggest that the maximum DOI changes significantly when the RS conductivity changes, Fig. 7. While ranges of over half a kilometer may be achieved if the conductivity is low (1×10^{-4} S/m), the signal will not propagate more than 100 m to 200 m in higher conductivity (1×10^{-3} S/m) conditions. It is worth noting that at a certain point, higher conductivities of the bounding reservoirs can result in a greater DOI. This is because while the signal attenuates more before reaching the RS, once inside the channel the higher conductivity of the reservoirs will be more efficient at containing the signal inside the RS, and therefore, the signal will experience less attenuation.

For comparison purposes, the attenuation rate (dB/100

Table 3 *Theoretical and simulated attenuation rate and maximum DOI as a function of RS conductivity. The wavelength used was 10 m.*

	Attenuation Rate (dB/100 m)			Theoretical Attenuation (dB/100 m)	Maximum DOI (km)		
RS Conductivity (S/m)	Scenario 1a	Scenario 1b	Scenario 1c	RS	Scenario 1a	Scenario 1b	Scenario 1c
1E-04	-17	-20	-34	-7	0.72	0.72	0.52
5E-04	-46	-49	-59	-37	0.26	0.3	0.29
1E-03	-82	-84	-95	-73	0.15	0.17	0.15

m) was calculated from the results and compared to what the attenuation rate would be if the wave was propagating entirely through the RS, Table 3. The results show that the attenuation obtained is higher than through a pure RS, but much lower than through the reservoir (data not shown). This confirms that the signal is indeed propagating mostly through the RS but is sensitive to the bounding reservoirs.

Another parameter evaluated was wellbore fluid conductivity because this can be controlled up to some degree during real life operations. For that purpose, the conductivity of the wellbore fluid was increased by two orders of magnitude. The results show that such a change in conductivity results in only 2 dB to 3 dB of additional attenuation, Fig. 8. Therefore, not a lot of effort should be put on controlling wellbore conductivity when conducting field experiments.

The final parameter tested was changing the ε of the wellbore fluid. For all simulations presented so far, the ε of the wellbore fluid has been 80 — roughly the same as water. Changes in ε create reflections at the interface that in turn result in additional attenuation. At first it might seem like matching the wellbore fluid's ε to that of the formation should therefore reduce attenuation and increase maximum DOI. Consequently, a smaller ε results in larger dipole antennas for the same frequency such that the antenna center ends up being further away from the RS reservoir B interface. The results showed a much higher attenuation when the ε was matched to the reservoir (data not shown).

Conclusions

The proximity sensing method had been previously demonstrated through qualitative numerical simulations and laboratory experiments. This study shows for the first time that it is possible to propagate high frequency signals (MHz) for several hundreds of meters in the presence of RSs bounded by conductive reservoirs. These findings, together with previous verification of the sensitivity of this approach to saturation changes in the bounding reservoirs, as proximity sensing paves the way for a new direction in high resolution EM surveys. The results presented here may serve as a guide to future field testing and the development of the technique and associated hardware. Some general recommendations for the implementation of this approach include:

- Generally lower frequencies are preferred and will result in increased DOI. It is, however, recommended to operate at frequencies that result in wavelengths in the RS equivalent to one to two times the thickness of that layer.
- The distance between the antenna and the RS reservoir B interface is crucial and every effort should be made to position the tool as close as possible to the interface. Smaller tools are also preferred.
- There is a tradeoff between reservoir conductivity and signal attenuation. More conductive reservoirs will increase the attenuation signal before it enters the RS, but once inside, higher conductivity reservoirs will be more efficient at containing the signal within the channel, and therefore, the signal will experience less attenuation while propagating through the RS.
- The electric conductivity of the RS has a very significant impact on the maximum DOI. Therefore, it is worth putting forth a significant effort to narrow down its value as much as possible. Since the RS is a natural layer, variations are expected. Determining a conductivity range would therefore be useful.
- Wellbore conductivity has a minimal effect, and therefore, it is not worth trying to reduce it. The ε of the fluid could have a greater impact, but at least in the configuration studied, high ε — such as water — yields better results than lower values — such as hydrocarbons.
- Some of these recommendations are only valid for a dipole antenna, and the optimal conditions may be different for other types of antennas.

Acknowledgments

The authors would like to thank the management of Saudi Aramco for their support and permission to publish this article.

This article was presented at the SPE Kingdom of Saudi Arabia Annual Technical Symposium and Exhibition, Dammam, Saudi Arabia, April 16-18, 2019.

References

1. Pathak, R.K. and Bakar, R.: "Estimating Saturation Changes from 4D Seismic: A Case Study from Malay Basin," IPTC paper 16910, presented at the International Petroleum Technology Conference, Beijing, China, March 26-28, 2013.
2. Tolstukhin, E., Lyngnes, B. and Sudan, H.H.: "Ekofisk 4D Seismic — Seismic History Matching Workflow," SPE paper 154347, presented at the SPE EUROPEC/EAGE Annual Conference, Copenhagen, Denmark, June 4-7, 2012.
3. Kelamis, P.G. and Uden, R.C.: "4D Seismic Aspects of Reservoir Management," OTC paper 8293, presented at the Offshore Technology Conference, Houston, Texas, May 5-8, 1997.
4. Denney, D.: "Saturation Mapping from 4D Seismic Data in the Statfjord Field," *Journal of Petroleum Technology*, Vol. 52, Issue 11, November 2000, pp. 38-40.
5. Marvillet, C., Al-Mehairi, Y.S., Shuaib, M., Al-Shaikh, A., et al.: "Seismic Monitoring Feasibility on Bu-Hasa Field," IPTC paper 11640, presented at the International Petroleum Technology Conference, Dubai, UAE, December 4-6, 2007.
6. Chen, G., Wrobel, K., Tiwari, A., Zhang, J., et al.: "4D Seismic in Carbonates: From Rock Physics to Field Examples," IPTC paper 12065, presented at the International Petroleum Technology Conference, Kuala Lumpur, Malaysia, December 3-5, 2008.
7. Marsala, A.F., Al-Ruwaili, S.B., Sanni, M.L., Shouxiang, M.M., et al.: "Crosswell Electromagnetic Tomography in Haradh Field: Modeling to Measurements," SPE paper 110528, presented at the SPE Annual Technical Conference and Exhibition, Anaheim, California, November 11-14, 2007.
8. Colombo, D., McNeice, G.W. and Kramer, G.: "Sensitivity Analysis of 3D Surface Borehole CSEM for a Saudi Arabian Carbonate Reservoir," *Society of Exploration Geophysicists Technical Program Expanded Abstracts*, 2012.
9. Aziz, A.A., Strack, K. and Hanstein, T.: "Surface-to-Borehole

TEM for Reservoir Monitoring," SEG paper 2011-1882, presented at the Society of Exploration Geophysicists Annual Meeting, San Antonio, Texas, September 18-23, 2011.

10. Marsala, A.F., Buali, M., Al-Ali, Z., Shouxiang, M.M., et al.: "First Borehole to Surface Electromagnetic Survey in KSA: Reservoir Mapping and Monitoring at a New Scale," SPE paper 146348, presented at the SPE Annual Technical Conference and Exhibition, Denver, Colorado, October 30-November 2, 2011.
11. Marsala, A.F., Lyngra, S., Widjaja, D.R., Laota, A.S., et al.: "Fluid Distribution Interwell Mapping in Multiple Reservoirs by Innovative Borehole to Surface Electromagnetic: Survey Design and Field Acquisition," IPTC paper 17045, presented at the International Petroleum Technology Conference, Beijing, China, March 26-28, 2013.
12. Felix Servin, J.M.: "Monitoring Water Flood Front Movement by Propagating High Frequency Pulses through Subsurface Transmission Lines," SPE paper 191874, presented at the SPE Asia Pacific Oil and Gas Conference and Exhibition, Brisbane, Australia, October 23-25, 2018.
13. Felix Servin, J.M., Ellis, E.S. and Schmidt, H.K.: "Proximity Sensing: A Novel Approach to Reservoir Saturation Monitoring Using High Frequency Electromagnetic Pulses," SPE paper 187282, presented at the SPE Annual Technical Conference and Exhibition, San Antonio, Texas, October 9-11, 2017.
14. Felix Servin, J.M., Schmidt, H.K. and Ellis, E.S.: "Improved Saturation Mapping Using Planar Transmission Lines and Magnetic Agents," SPE paper 181343, presented at the SPE Annual Technical Conference and Exhibition, Dubai, UAE, September 26-28, 2016.
15. Schmidt, H.K., Felix Servin, J.M. and Ellis, E.S.: "Experimental Verification of a New Approach to Long-Range EM Imaging," SPE paper 192333, presented at the SPE Kingdom of Saudi Arabia Annual Technical Symposium and Exhibition, Dammam, Saudi Arabia, April 23-26, 2018.

About the Authors

Jesus M. Felix Servin

M.S. in Chemical and Biological Engineering, King Abdullah University of Science and Technology

Jesus M. Felix Servin joined the Reservoir Engineering Technology Division of Saudi Aramco's Exploration and Petroleum Engineering Center – Advanced Research Center (EXPEC ARC) in February 2012. His focus is on the development of electromagnetic methods and nanoparticle-based contrast agents for reservoir characterization and monitoring. Jesus's role has been instrumental in the development and deployment of the Magnetic Nano-Mappers project, including hardware design and in-house fabrication, instrumentation, computer programming, and data processing.

Jesus' interests include the development of nanoscale strategies for reservoir illumination and electromagnetic methods for reservoir description and monitoring.

He received his B.S. degree in Engineering Physics from Instituto Tecnologico y de Estudios Superiores de Monterrey, Monterrey, Mexico, and an M.S. degree in Chemical and Biological Engineering from King Abdullah University of Science and Technology, Thuwal, Saudi Arabia.

Dr. Max Deffenbaugh

Ph.D. in Electrical Engineering, Massachusetts Institute of Technology

Dr. Max Deffenbaugh joined Aramco Services Company in 2013, where he leads the Sensors Development Team at the Houston Research Center.

His previous experience includes 16 years at ExxonMobil, working on seismic signal processing, simulation, and inverse problems in process geology, computational rock physics, and the development of downhole sensor networks. Max has also developed wireless telemetry systems for biologists to record muscle and brain signals from animals in their natural environments.

In 1997, he received his Ph.D. degree in Electrical Engineering from the Massachusetts Institute of Technology/Woods Hole Oceanographic Institution Joint Program, Cambridge, MA.

Robert W. Adams

M.S. in Electrical Engineering, University of Texas at Austin

Robert W. Adams is an Electrical Engineer in the Sensors Development Team for the Aramco Services Company – Houston Research Center. His research interests include ultrasonics, electromagnetics, signal processing, and electronics design. Robert's previous experience includes being involved in the design and development of novel sensors for upstream oil and gas challenges.

In 2012, Robert received his M.S. degree in Electrical Engineering from the University of Texas at Austin, Austin, TX.

Dr. Val Riachentsev

Ph.D. in Mechanical Engineering, Novosibirsk State Technical University

Dr. Val Riachentsev is an Electrical Engineer working on the Sensors Development Team in the Aramco Services Company Houston Research Center.

His previous experience includes work in the electromagnetic fields simulation, design and development of electromagnetic sensors and drives, power electronics, acoustic and seismic sources operating in harsh environments.

In 1974, Val received his M.S. degree in Electrical Engineering, and in 1982, he received his Ph.D. degree in Mechanical Engineering, both from the Novosibirsk State Technical University, Novosibirsk, Russia.

Development of a Robust and Nondestructive Microscopic Phase Behavior Monitoring Method to Screening High Performance Surfactants

Marwah M. AlSinan, Dr. Hyung T. Kwak, Alhasan B. Fuseni, and Jun Gao

Abstract /

Surfactant screening for enhanced oil recovery involves studies of fluid-fluid and fluid-rock interactions to optimize the surfactant formulation for the reservoir of interest. In this article, we present a suite of advanced low field nuclear magnetic resonance (NMR) technologies capable of monitoring the phase behavior microstructure of fluid mixtures developed for high salinity and high temperature conditions. An anionic and nonionic-anionic surfactant mixture were selected since they were developed for high salinity and high temperature reservoirs.

The surfactant performance was monitored over several months using phase behavior tests. For both surfactants, salinity scans were carried out using synthetic seawater. In addition to visual inspection, a set of NMR measurements, including average and spatial T_2, were conducted to detect dispersed phases throughout the aging process. Also, 1D diffusivity and 2D T_2-diffusivity (T_2-D) experiments were carried out to identify microstructural changes.

The anionic surfactant formed an emulsion right after agitation while the nonionic-anionic surfactant took more than a month to form a stable emulsion. The 2D T_2-D experiments showed different diffusion coefficients for oil and water. For the nonionic-anionic mixture, oil and water diffusivities were similar to the unmixed oil and water diffusivities. While the diffusivities for the nonionic-anionic mixture increased gradually over a month, until they reached the same value, the diffusivities for the anionic surfactant reached the same value on the second day. Spatial T_2 measurements confirmed the stability of the formed emulsions.

Low field NMR techniques provide a nondestructive and robust method of monitoring surfactant performance, including dispersed volumes, emulsion stabilization time, emulsion type, and surfactant efficiency. In addition, they are capable of microscopic phase behavior monitoring, which is not possible with conventional visual monitoring techniques.

Introduction

Evaluating the emulsions and microemulsion's stabilization mechanisms and microstructural properties is of great interest to the enhanced oil recovery processes. The microstructure of an emulsion has a significant impact on its rheological properties, which would affect the sweep efficiency and recovery of a chemical flood. Also, the process of chemical design would be significantly improved when the different factors that affect an emulsion stabilization are well understood.

Materials and Methods

Materials

Filtered crude oil was used in all of the experiments. Synthetic seawater was used in all of the samples. For the first set, the brine contains ions such as Na^+, Ca^{+2}, Mg^{+2}, Cl^-, SO_4^{-3}, and HCO_3^-, while the second set of brines contain Na^+, Ca^{+2}, Mg^{+2}, and Cl^- only. For the first set, the brine salinity was varied from 0 wt% to 20 wt%. Each sample contained 0.5% of a surfactant, which is a mixture of a nonionic alcohol and an anionic surfactant containing sulfonate. A 5 mL:5 mL water-oil ratio was maintained in all of the samples.

For the second batch, the ionic strength was varied from 2.5 wt% to 9 wt%. Each sample contained 2.4% surfactant, which is a mixture of two anionic sulfonate surfactants. A 3 mL:3 mL water-oil ratio was maintained in all of the samples.

Samples Preparation

The methodology of sample preparation for phase behavior studies and surfactant screening has been reported in many articles[1, 2]. For the current study, samples were prepared in the calibrated conical vials to estimate oil and water solubility over time. Both sample sets were covered with Teflon tape and plastic caps to prevent any evaporation. Once the samples were prepared, they were hand shaken for 1 minute. The first batch was placed in an oven at 95 °C while the second set was kept at room temperature, 25 °C. The shaking process was repeated

every 24 hours to encourage emulsion formation.

Once the samples were prepared, initial readings of the oil and water volumes were recorded before agitating the samples. For the first batch, volumetric readings were noted after the samples were shaken and cooled to account for heat-related fluid expansion. Also, the oil and water phases returned to their original volumes shortly after agitation and formed a rigid oil-water contact in all of the first batch samples.

For the second set, opaque macroemulsions were suspected following agitation of the samples. Also, a middle phase was observed in several samples. Nuclear magnetic resonance (NMR) measurements were conducted on the emulsified and stabilized samples to evaluate any shaking-related changes.

NMR Measurements

A low field NMR relaxometer, with 12 MHz resonance frequency for H^1, and equipped with gradient coils of 25 Gauss/cm maximum strength, was utilized for the current study. The relaxometer was originally designed for rock core plug studies.

Increasing the temperature would increase the internal energy of the system, which is proportional to the diffusivity[3]. To compare results from the NMR tests on the different samples, all NMR measurements were conducted at room temperature.

Factors that Could Affect Experiments and the Sample's Quality

Shaking. Shaking encourages the mixing of the two phases and the forming of more stable emulsions. In addition, the applied stress and strain rates during shaking can affect the volume of the dispersed phase in the emulsion[4]. Since the microemulsion forms as a result of the thermodynamic state of the system, however, shaking would not have a significant impact on its properties.

For the current study, hand shaking was selected since the sample volume was small. Although the hand shaking is inconsistent, in terms of applied stress and its frequency, we have adapted it as the method of choice for the mixing process because the end goal of the current study was to obtain microemulsions. For NMR measurements, shaking the samples before the test had an impact on spatial T_2 only, Fig. 1. On the other hand, T_2 and diffusion tests were not affected by the shaking. This is probably

Fig. 1 *T_2 and diffusion and spatial T_2 for the surfactant formulation sample with 7 wt% salinity before and after shaking on the 7th and 8th day, respectively. The sample and measurements were kept at room temperature.*

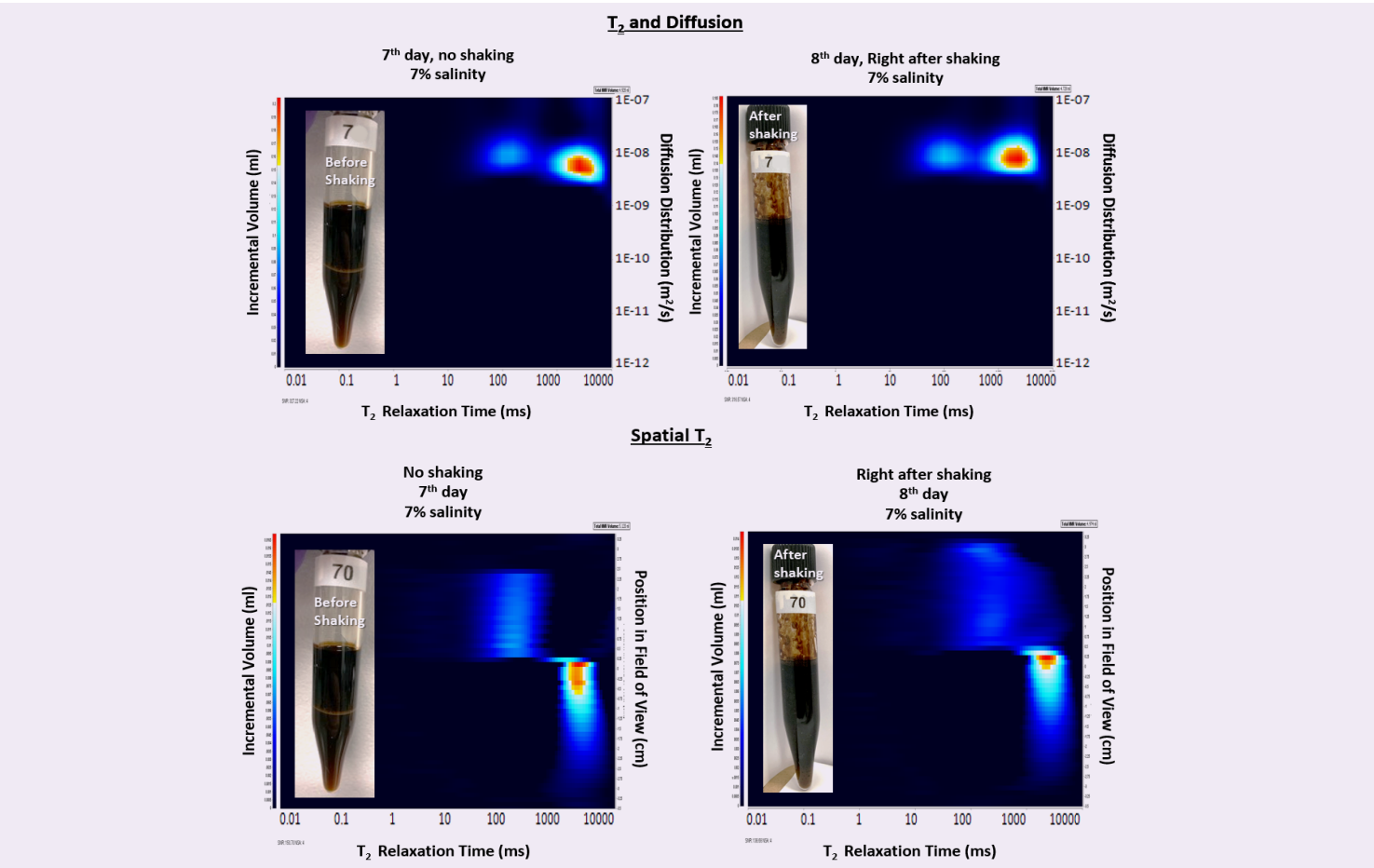

due to the sensitivity limitation for the dispersed phase volumes, and the diffusivity measurement by the low field NMR instrument. These measurements can be repeated on a NMR relaxometer optimized for emulsion droplet measurements with higher sensitivity, and better applied gradient characteristics to confirm this finding.

Measurement Frequency. Through the series of conducted tests in this work, NMR measurements were not taken at consistent time intervals. NMR tests will be conducted at shorter intervals in the future to confirm the results.

Results and Discussion

Alcohol and Sulfonate Surfactant Samples

During the first month following preparation of the samples, whenever the samples were agitated, the emulsion would separate very quickly into the free oil and brine phases. Emulsion breakdown could be due to many reasons, which includes: pH, ionic strength, rheology, and droplet size[5, 6]. Also, to stabilize an emulsion, surfactants have to form barriers around droplets to prevent them from collapsing during collision with neighboring droplets. These energy barriers could be physical — steric forces — or electric repulsive forces in ionic surfactants[7]. For many surfactants, the energy barriers require aging and frequent mixing between the two phases to reform more stable droplets[8].

Figure 2 shows a series of T_2 and diffusion tests, along with spatial T_2 measurements for an oven aged sample with 20 wt% salinity that were taken over time. The 12 days of measurement shows that the diffusion of oil and brine is very similar to the original values for the

Fig. 2 Evolution of T_2 and diffusion and spatial T_2 tests for the alcohol and sulfonate surfactant sample with 20 wt% salinity that was aged in an oven at 95 °C. For all tests, the sample was agitated before taking the measurements. Although spatial T_2 for 12 days is missing, it is likely similar to the one at 29 days and at 5 days in Fig. A3 since emulsions at that time would break before the test was completed.

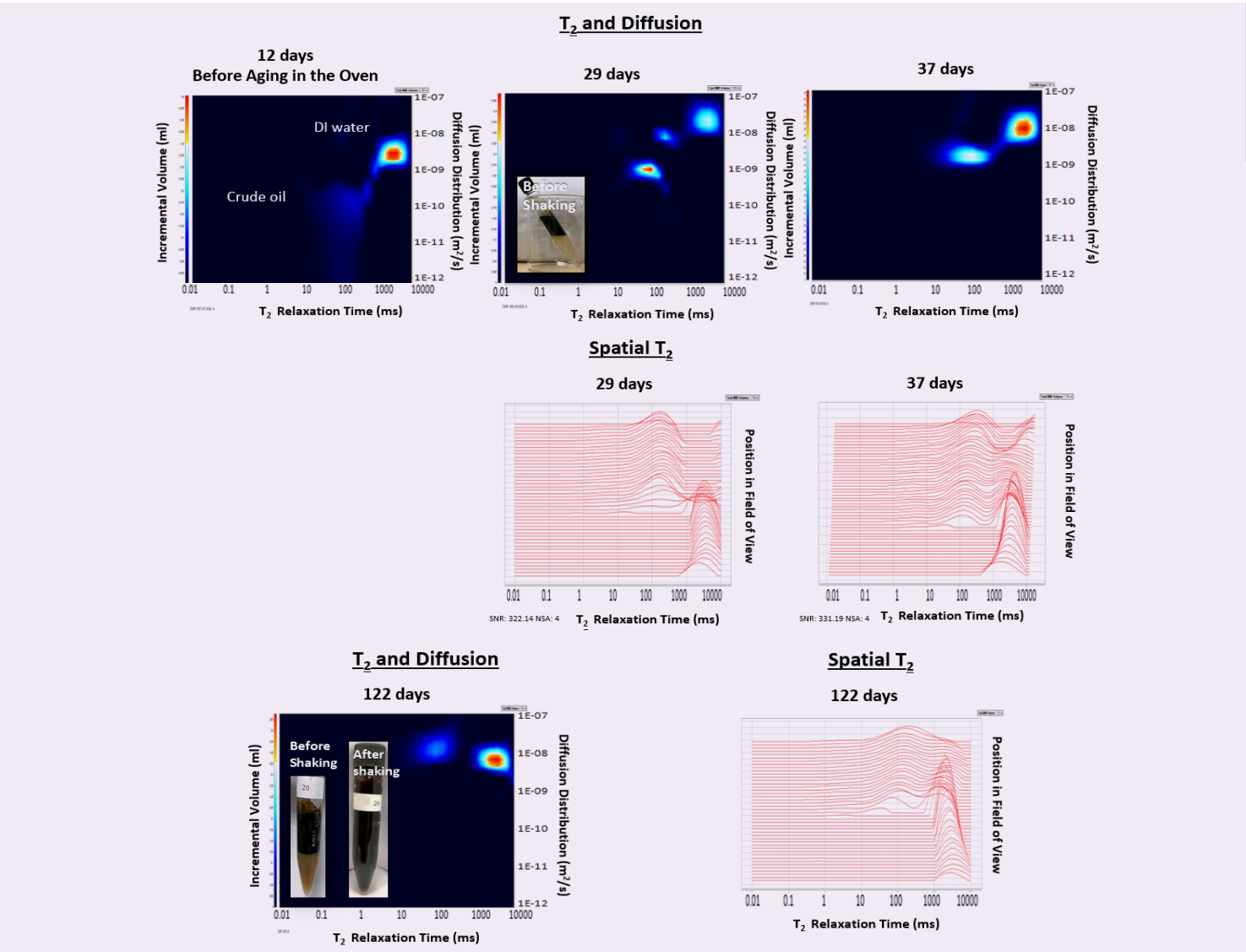

Fig. 3 *T_2 and diffusion and spatial T_2 for crude oil and DI water in separate bottles, right after mixing crude oil and DI water, and after 35 days of aging at room temperature. For tests conducted right after mixing and for the aged sample, the sample was agitated before taking the measurements.*

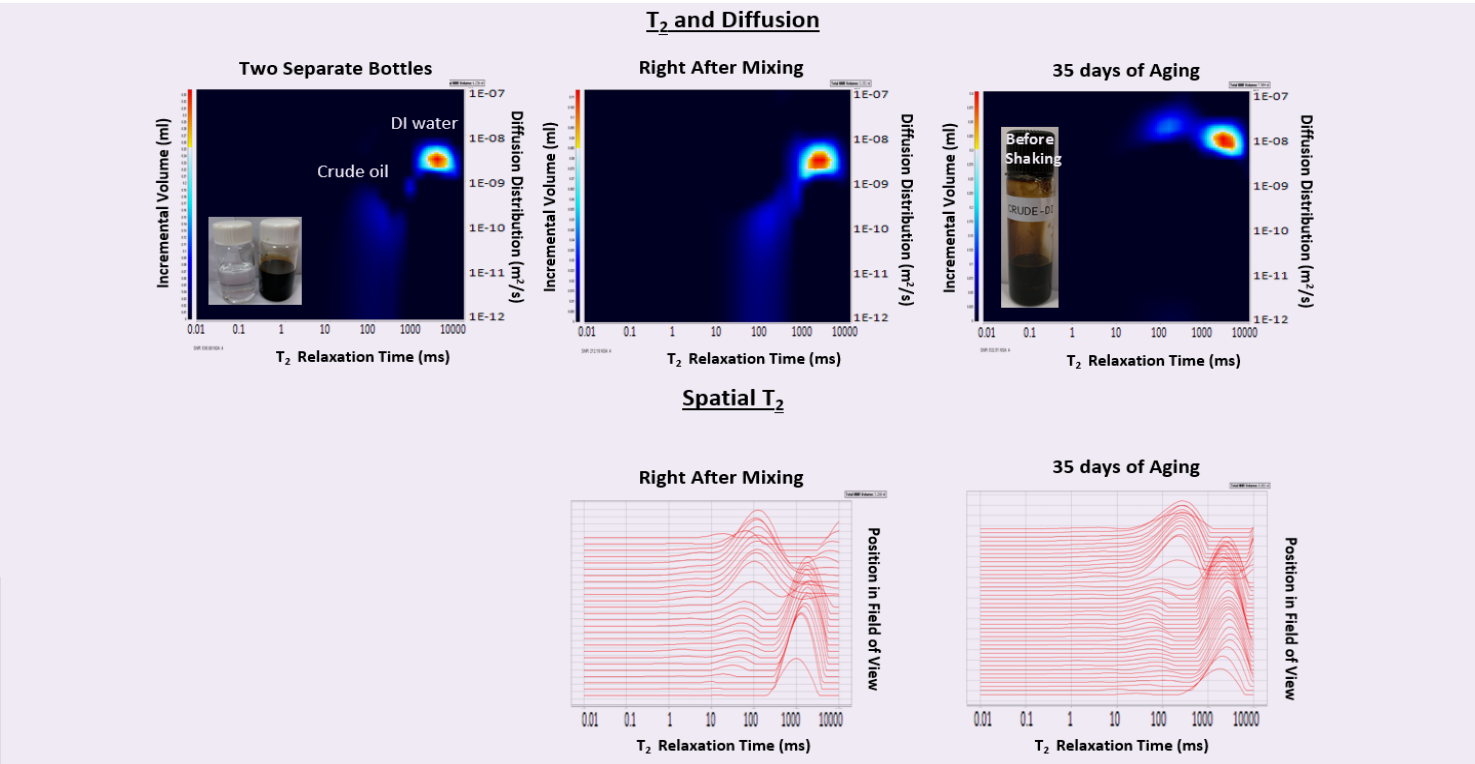

unmixed crude oil and deionized (DI) water in Fig. 3. In the subsequent measurements, the oil diffusion increases at a faster rate than the brine's. In the 122 day measurement, both diffusions settle around the same value, which is similar to the observation of DI water and crude oil emulsion after 35 days of aging in Fig. 3.

In addition, on day 37, the spatial T_2 measurement shows water dispersed in the oil phase, which could not be detected previously since the emulsion broke down before the test was completed. Figures 4 and 5 show similar observations for tests on the samples with 0 wt% and 20 wt% salinities, which were aged at room temperature. Although the presence of oil could be detected visually on day 37, oil dispersion in the water phase did not show up in the spatial T_2 measurement. This could be due to the oil relaxation signal being overwhelmed by the brine's, since water has a higher volume percentage in an oil-water emulsion.

In the T_2-D measurements, the self-diffusivity of the droplets could not be measured with certainty due to many reasons, including the sensitivity for a small volume and the self-diffusivity of the droplet being lower than the minimum detectable diffusivity of our instrument. Therefore, in the T_2-D measurements, the diffusivity distribution could be the net result of the dispersed particles and continuous phase diffusions. In addition, the spatial T_2 and the T_2-D measurements for a small amount of emulsion are limited by technical limitations, due to the homogeneity of the applied gradient field and the inaccuracy of volumetric information by the 2D inversion process, respectively. Therefore, the data from these two measurements are used for qualitative analysis only for the current study. On the other hand, the data from the average T_2 and 1D diffusivity measurements, which do not have these issues, would be used for quantitative analysis in future studies.

In Fig. 2, the changes in diffusion behavior could be related to the development of energy barriers by the surfactants around the dispersed particles. During the first days, collision between emulsion droplets could have resulted in coalescence due to weak barriers, which explains the accelerated breakdown of the emulsion. Also, the inability of the emulsion to be stabilized could justify the restriction of particle Brownian motion to their respective bulk phases. This would have resulted in maintaining the original diffusion for oil and brine. Also, during the early periods after sample preparation, the aqueous phase was analyzed using liquid NMR and mass spectroscopy tests, which did not show any dispersed oil particles, which are not presented in the current manuscript.

In the spatial T_2 test on day 37, the emulsion was becoming more stable, which correlates with the development of barriers. As a result, the dispersed particles would have more freedom than before to diffuse in the opposite phase, which could explain the increase in diffusion distribution of both phases. Consequently, more tests would have to be conducted

Fig. 4 *T_2 and diffusion and spatial T_2 for the alcohol and sulfonate surfactant samples with 0 wt% salinity that were aged at room temperature. For both the five and 43-day tests, the sample was agitated before taking the measurements.*

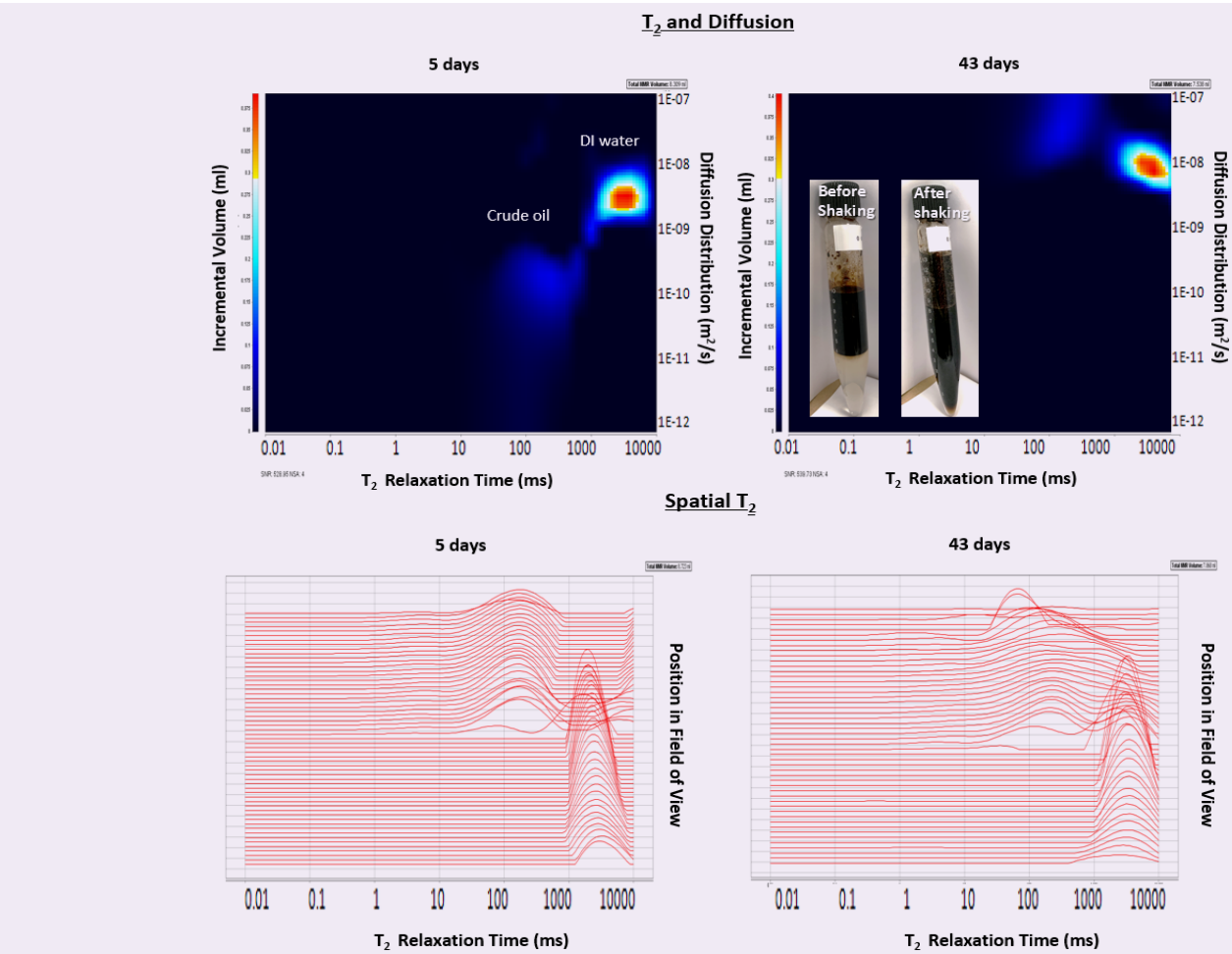

to support the aforementioned hypothesis. This includes the measurement of particle size changes over time in addition to the energy barrier measurements, such as the evaluation of the double layer in ionic solutions using Zeta potential[7]. Also, the aforementioned hypothesis does not explain the difference in diffusion acceleration between the oil and brine.

Surfactant Formulation Samples

This sample set formed an emulsion right after the first agitation took place. The emulsion was more stable than the alcohol and sulfonate surfactant set. Visual inspection indicated the formation of water in oil and oil in water emulsions and a middle layer of 0.5 ml to 1 ml thickness. The water in oil emulsion was confirmed in the spatial T_2 test while the oil in water emulsion could not be detected due to the sensitivity issue discussed in the alcohol and sulfonate surfactant sample set, Fig. 6. Also, Fig. 7 shows that oil and brine diffusivity increased to the same value very quickly starting from the second day, which is similar to the diffusivity behavior for the first sample set on day 122. This could indicate the fast development of barriers around dispersed particles by this specific surfactant.

Conclusions

We presented a workflow for monitoring crude oil-brine surfactant systems phase behavior, which incorporates a suite of advanced low field NMR measurements with conventional visual inspection of bottle tests. The NMR tests provide a nondestructive and robust method of monitoring surfactant performance in detail, which conventional visual inspection could not. The advanced NMR techniques, such as the 2D T_2-D and the spatial T_2 measurement can be used to track emulsion stabilization, and to confirm emulsion structure and type, respectively.

For future studies, additional advanced tests such as particle size distribution and Zeta potential will be conducted to support the findings from the NMR experiment. Also, quantitative analysis will be carried out on the conducted NMR tests.

Acknowledgments

The authors would like to thank the management of Saudi

Fig. 5 *T_2 and diffusion and spatial T_2 for the alcohol and sulfonate surfactant samples with 20 wt% salinity that were aged at room temperature. For both the 12 and 47-day tests, the sample was agitated before taking the measurements. Although spatial T_2 for 12 days is missing, it is likely similar to the one at 29 days in Fig. 1 and at 5 days in Fig. A3, since emulsions at that time would break down before the test is completed.*

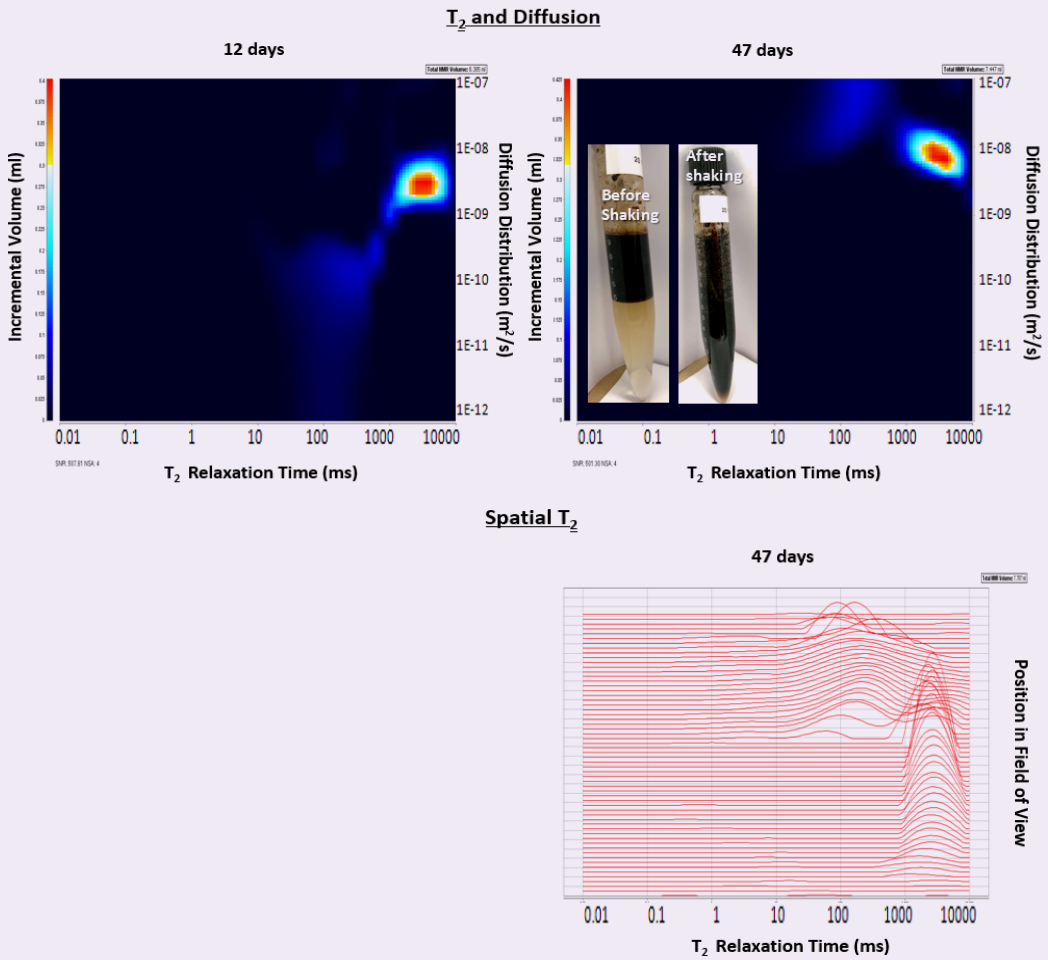

Fig. 6 *T_2 and diffusion and spatial T_2 tests for the surfactant formulation sample with 9 wt% salinity that was aged at room temperature. The sample was agitated before taking the measurements.*

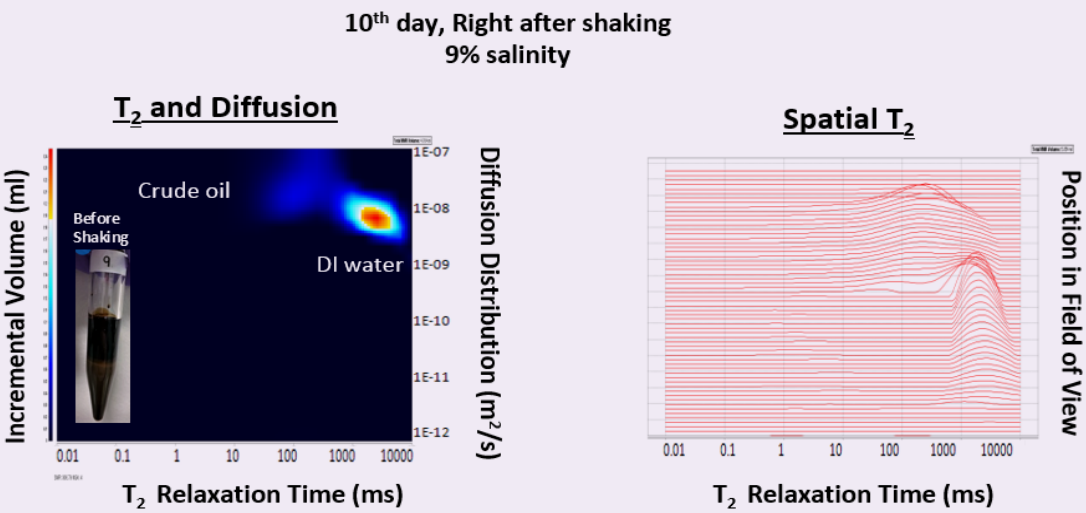

Fig. 7 *T_2 and diffusion for surfactant formulation sample with salinities 2.5%, 7%, 8%, and 9% that were aged at room temperature.*

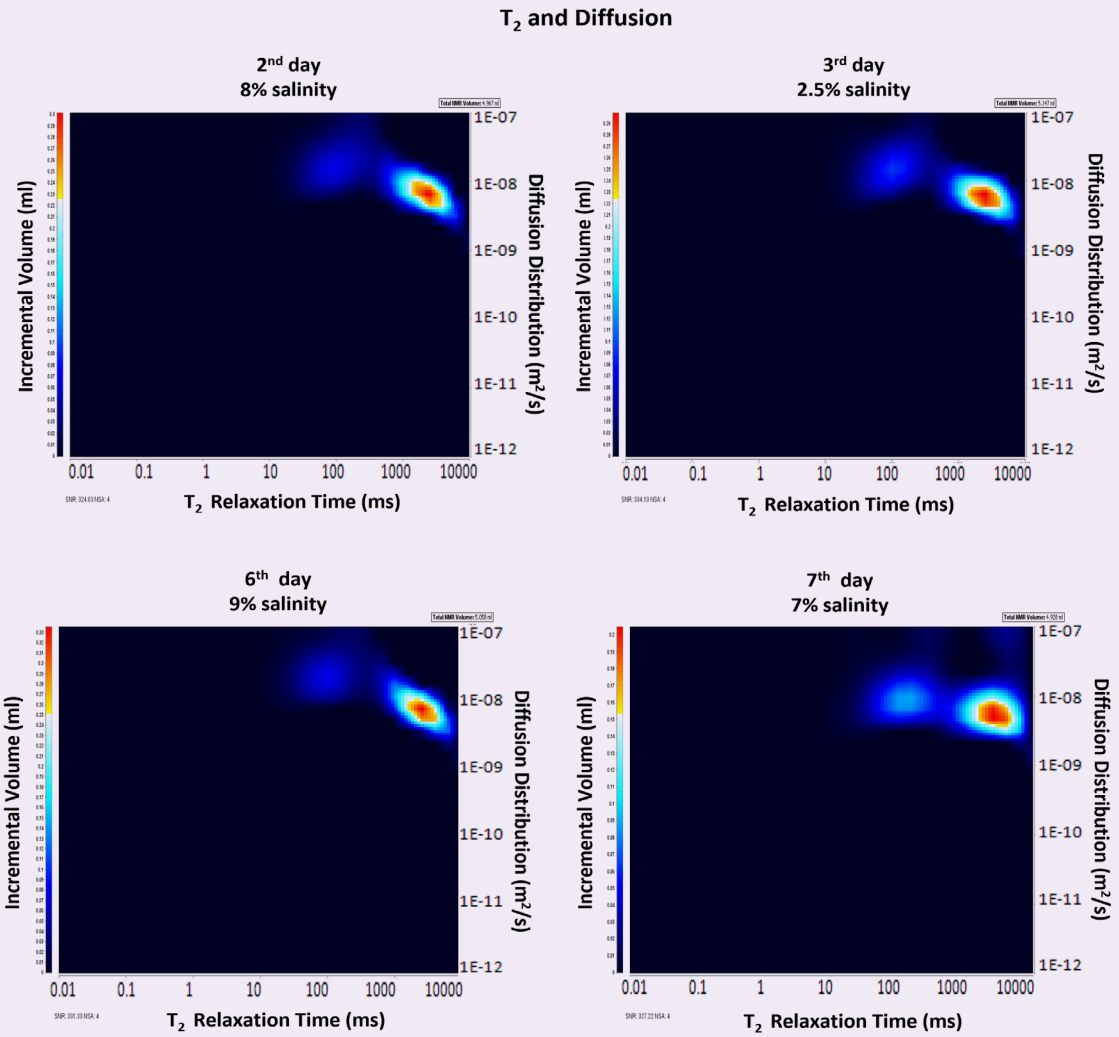

Aramco for their support and permission to publish this article. The authors would also like to thank Mustafa Satrawi for assisting in the preparation of the samples.

This article was presented at the SPE Kingdom of Saudi Arabia Annual Technical Symposium and Exhibition, Dammam, Saudi Arabia, April 16-18, 2019.

References

1. Levitt, D., Jackson, A., Heinson, C., Britton, L.N., et al.: "Identification and Evaluation of High-Performance EOR Surfactants," *SPE Reservoir Evaluation & Engineering*, Vol. 12, Issue 2, April 2009, pp. 243-253.
2. Flaaten, A., Nguyen, Q.P., Pope, G.A. and Zhang, J.: "A Systematic Laboratory Approach to Low-Cost, High Performance Chemical Flooding," SPE paper 113469, presented at the SPE Symposium on Improved Oil Recovery, Tulsa, Oklahoma, April 20-23, 2008.
3. Stilbs, P.: "Fourier Transform Pulsed Gradient Spin-Echo Studies of Molecular Diffusion," *Progress in Nuclear Magnetic Resonance Spectroscopy*, Vol. 19, Issue 1, 1987, pp. 1-45.
4. Peña, A.A., Hirasaki, G.J. and Miller, C.A.: "Chemically Induced Destabilization of Water-in-Crude Oil Emulsions," *Industrial & Engineering Chemistry Research*, Vol. 44, Issue 5, 2005, pp. 1139-1149.
5. Lyklema, J.: *Fundamentals of Interface and Colloid Science*, 1st edition, Academic Press, NY, 2005, 844 p.
6. Schramm, L.L.: *Emulsions: Fundamentals and Applications in the Petroleum Industry*, ACS Advances in Chemistry Series 231, American Chemical Society, Washington, D.C., 1992, 428 p.
7. Schramm, L.L.: *Emulsions, Foams, and Suspensions: Fundamentals and Applications*, Wiley-VCH, 2005, 463 p.
8. Abbott, S.J.: *Surfactant Science: Principles & Practice*, Destech Publications, 2017, 198 p.

About the Authors

Marwah M. AlSinan

M.S. in Petroleum Engineering, Imperial College London

Marwah M. AlSinan is a Petroleum Engineer with the Reservoir Engineering Technology Division of Saudi Aramco's Exploration and Petroleum Engineering Center – Advance Research Center (EXPEC ARC). Currently, she is working in reservoir engineering research with a focus on in situ monitoring and modeling using nuclear magnetic resonance technology.

Marwah's experience includes working in oil reservoir management and gas simulation at 'Uthmaniyah, where she participated in integrated reservoir studies of the Haradh, Jufain and Waqar fields.

In 2013, Marwah received her B.S. degree in Petroleum Engineering from Pennsylvania State University, State College, PA, and in 2017, she received her M.S. degree in Petroleum Engineering from Imperial College London, London, U.K.

Dr. Hyung T. Kwak

Ph.D. in Physical Chemistry, Ohio State University

Dr. Hyung T. Kwak joined Saudi Aramco in April 2010 as a Petroleum Engineer with Saudi Aramco's Exploration and Petroleum Engineering Center – Advance Research Center (EXPEC ARC). He had been a member of the Pore Scale Physics focus area (2010 to 2012) and SmartWater Flooding focus area (2013 to 2014) of the Reservoir Engineering Technology Division. Currently, Hyung is a focus area champion of the Pore Scale Physics focus area. His main research focus is seeking deeper understanding of fluid-rock interaction in pore scale of the Kingdom's reservoirs.

Since joining Saudi Aramco in 2010, Hyung has been involved with various improved oil recovery and enhanced oil recovery (EOR) research projects, such as SmartWater Flooding, carbon dioxide EOR, and chemical EOR. Prior to joining Saudi Aramco, Hyung was a Research Scientist at Baker Hughes, with a main area of research related to nuclear magnetic resonance (NMR)/magnetic resonance imaging technology.

In 1996, Hyung received a B.S. degree in Chemistry from the University of Pittsburgh, Pittsburgh, PA, and in 2001, he received his Ph.D. degree in Physical Chemistry from Ohio State University, Columbus, OH.

Before moving into the oil and gas industry, Hyung was involved — as a postdoctoral fellow for 2 years — in a project developing the world's largest wide bore superconducting magnet NMR spectrometer, 900 MHz, at the National High Magnetic Field Laboratory.

He has more than 100 publications, including peer-reviewed articles and patents.

Alhasan B. Fuseni

M.S. in Petroleum Engineering, King Fahd University of Petroleum and Minerals

Alhasan B. Fuseni joined Saudi Aramco in 2006 and is a member of the Chemical Enhanced Oil Recovery (EOR) team of the Exploration and Petroleum Engineering Center – Advanced Research Center (EXPEC ARC). Prior to joining Saudi Aramco, he worked for the King Fahd University of Petroleum and Minerals (KFUPM) Research Institute as a Research Engineer, and for Hycal Energy Research, Calgary, Canada, as an EOR technologist. Alhasan has taught an in-house course on core flooding applications in chemical EOR at EXPEC ARC, and he teaches the chemical EOR section of the course on EOR at Saudi Aramco's Upstream Professional Development Center. He has authored and coauthored several papers in petroleum engineering and is currently serving as a reviewer for Elsevier's *Journal of Petroleum Science and Engineering*.

Alhasan received both his B.S. and M.S. degrees in Petroleum Engineering from KFUPM, Dhahran, Saudi Arabia, in 1985 and 1987, respectively.

Jun Gao

M.S. in Petroleum Engineering, University of Calgary

Jun Gao joined Saudi Aramco in October 2015 and is currently working in Saudi Aramco's Exploration and Petroleum Engineering Center – Advanced Research Center (EXPEC ARC) as a Petroleum Scientist with the Reservoir Engineering Technology Division. Prior to joining Saudi Aramco, he worked as a Research Scientist on multiple advanced enhanced oil recovery (EOR) studies for oil companies at Tomographic Imaging and Porous Media Laboratory (TIPM lab) in Perm Inc. and the University of Calgary. Prior to that, Jun worked as a Petroleum Engineer on national chemical EOR research projects at the Geological Scientific Research Institute, Shengli Oil Field Company, and China Petroleum & Chemical Corporation (Sinopec).

He has over 25 years of research experience in special core analysis and EOR, including chemical, thermal, and carbon dioxide techniques, assisted by imaging technologies such as X-ray computer tomography and nuclear magnetic resonance imaging.

Jun received his B.S. degree in Physics from Shandong University, Shandong, China, his B.Eng. degree in Petroleum Engineering from the China University of Petroleum (East China), Qingdao, China, and his M.S. degree in Petroleum Engineering from the University of Calgary, Calgary, Alberta, Canada.

Pushing the Limits of Coiled Tubing to Address the Challenges of Matrix Stimulation in Multilateral Extended Reach Power Water Injectors

Hasan M. Al-Jassem, Naji K. Al-Salman, Rifat Said, Danish Ahmed, and Kaisar Al Hamwi

Abstract /

In carbonate reservoirs in the Middle East, power water injector wells are typically completed with long open hole laterals. The reservoir contact provides pressure support and enhances sweep efficiency in the low transmissibility reservoirs. Due to the wells' deviation and length, coiled tubing (CT) interventions are required to successfully enter and identify each lateral, as well as to remove formation damage by pumping the matrix stimulation treatment across entire laterals.

During such CT interventions, laterals are accessed thanks to a hydraulically operated lateral identification tool, while the stimulation treatment is pumped through a ball drop activated high-pressure jetting nozzle (HPJN). The lateral identification tool and HPJN are efficiently operated by monitoring downhole pressure values, both inside and outside of the bottom-hole assembly (BHA), in real time thanks to CT fiber optic telemetry. Those downhole pressure readings further assist in optimizing the pumping rate during the job, while keeping it below the fracturing pressure. Finally, the telemetry provides support for gamma ray logging, which facilitates depth control and lateral identification.

This study features an application history during which the matrix stimulation treatment was conducted in two separate CT runs for both laterals of the well. For the first run, the CT initially entered the motherbore (L-0) following the natural path of the well, whereas the lateral (L-1) was accessed by activating the lateral identification tool. The correct lateral entry was confirmed by matching the acquired gamma ray readings with reference logs. After successfully accessing L-1 and reaching its maximum depth, a ¾" ball was dropped to isolate the lateral identification tool and activate the HPJN for stimulation.

During the second run, as the CT entered L-0, gamma ray monitoring was used to confirm lateral accessibility. The stimulation treatment was pumped after reaching maximum depth and isolating the HPJN. During the stimulation of each lateral, 20% viscoelastic diverting acid was utilized for diverting from high intake zones, and 20% hydrochloric (HCl) acid to stimulate the damaged/tight zones.

This operation illustrates how downhole pressure gauge readings are used to sequentially operate the lateral identification tool efficiently and activate the HPJN, as well as to pump the matrix stimulation treatment below the fracturing pressure. Real-time gamma ray readings, meanwhile, are used for depth control and to correctly identify laterals.

Introduction

Water injector wells are typically drilled in the periphery of oil reservoirs. Water is injected into the underlying aquifer or sometimes into the oil-bearing zone to enhance sweep efficiency and limit the production decline by pressurizing those reservoirs.

In such formations, fractures and fissures are often present within the matrix, thereby generating dual porosity. As a result, when water is injected, it tends to flow through the pass of least resistance; that is, within fractures and fissures. This is a nondesireable situation, since it then bypasses sections of the matrix requiring pressure support.

The result is a nonhomogeneous injection that leaves entire sections of the reservoir unswept and can lead to hydrocarbons being unrecoverable with time. It is therefore of utmost importance to stimulate any zone with low intake, e.g., because of drilling mud damage, and ensure water is injected to its full potential so that hydrocarbon recovery can be made efficient.

Background

In this setting, since wells are typically completed as open holes, matrix acidizing by bullheading — injecting stimulation fluids from the surface — is often selected to perform the stimulation. This option is not adapted to multilateral wells because it is then impossible to know in which lateral the stimulation fluid is going when pumping. The situation becomes even more challenging with the fact that wellheads installed on these wells are limited to significantly low pressure, i.e., 2,500 psi. Although this pressure limitation can be mitigated by installing a tree

saver while bullheading the treatments, the horizontal nature of laterals calls for stimulating the wells at a higher rate so that the fluids can reach the total depth (TD) of the laterals. In practice, most often the stimulation fluid only reaches a certain lateral length, which leads to a noneffective stimulation treatment.

The proposed application study features a dual lateral extended reach power water injector well in need of a stimulation treatment. Although that well was like any other dual water injector well in the area in many respects, it was particularly long, with its two open hole laterals having a combined length topping 20,000 ft. It was also the first of its kind with such long laterals in the respective reservoir. As a solution to the aforementioned challenges, coiled tubing (CT) was chosen to maximize the chances to deliver a uniform treatment across each lateral.

It should be noted that CT typically buckles when run in the hole (RIH) in horizontal wells. This means that tagging TD to identify the lateral — as often done in conventional CT operations — should not be relied on, since the CT can lockup before reaching each lateral's TD, thereby preventing any lateral identification, and in turn, potentially leading to the stimulation of the wrong lateral[1].

To address those challenges, CT equipped with real-time downhole telemetry was utilized. It allowed identifying the accessed lateral correctly by matching the acquired readings of gamma ray with reference logs. It also facilitated the use of a lateral identification tool to successfully enter each lateral, as well as a ball drop activated high-pressure jetting nozzle (HPJN) to pump the stimulation fluids through the CT at higher pressure with a jetting effect. Downhole sensors of pressure and temperature located in the bottom-hole assembly (BHA) are used to this effect[2-4].

The reader will note that the use of CT with real-time telemetry does not guarantee by itself that the pipe will be able to reach the lateral's TD. It shall be complemented by enhanced reach methods — such as tapered pipe design, pumping of a friction reducer, or even use of tractors — to reach this end. Such units do enable the identification of accessed laterals, and in cases when the CT can only reach a certain depth, it allows pumping the treatment through the CT, anticipating those fluids would flow down to the noncovered CT depths, followed by reciprocating the remainder of the treatment across the interval that can be covered by the CT.

Well Information

Figure 1 is a schematic of the well under consideration, consisting of two horizontal laterals — the motherbore (L-0) and the lateral (L-1). The combined length of both laterals is more than 20,000 ft. Both are completed with a 6⅛" open hole. The L-0 open hole section is located below a 7" liner that runs down to 9,353 ft measured depth (MD), equivalent to 7,190 ft true vertical depth (TVD). Lateral L-1 was drilled through the 7" liner; the junction is located at 9,149 ft MD (7,169 ft TVD). The bottom-hole temperature for both laterals ranges from 100 °F to 110 °F.

Fig. 1 A wellbore schematic: The black path corresponds to the motherbore (L-0) and the red path to the lateral (L-1).

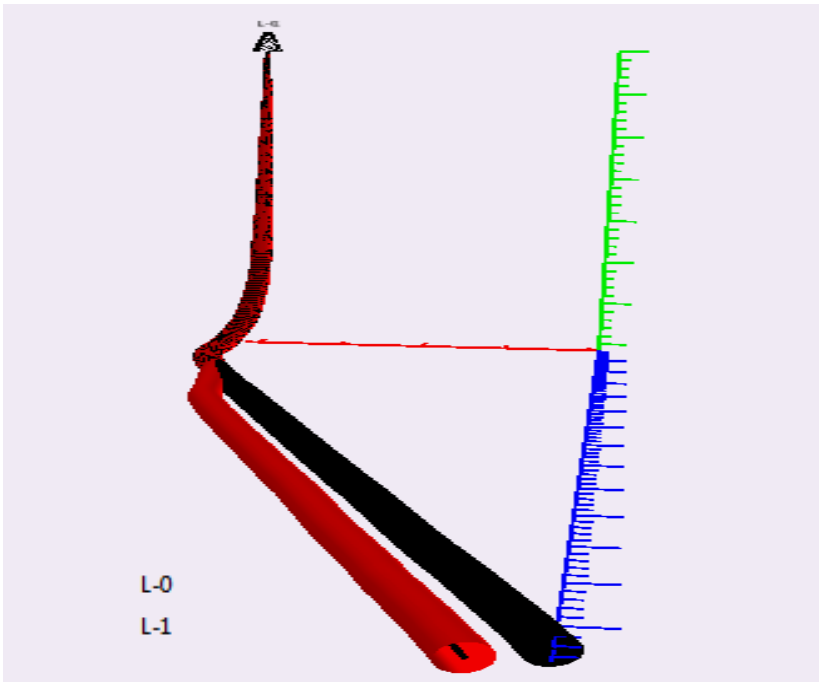

After the well was completed, an injectivity test was originally planned but never carried out, by fear that the mud present in the wellbore may cause more damage in the reservoir. Well displacement was therefore included when designing the intervention and later kept as a best practice for future similar operations. Taking into consideration that the reservoir was tight and damaged by drilling mud, a matrix stimulation was planned to increase the injection rate at lower wellhead pressures. Since the combined use of a conventional CT with a lateral identification tool could not guaranty lateral confirmation by simply tagging the lateral TD, CT enabled with real-time downhole readings was selected to deliver the treatment following the methodology previously described.

Fiber optics was selected as the telemetry link so that the crew also had access to distributed temperature sensing (DTS) during the operation. That information was planned to be used to optimize fluid placement during the stimulation phase of each lateral, provided that the CT was not getting stuck into the open hole section. This was a legitimate concern, as the CT needs to remain stationary for extended periods of time when performing DTS acquisition.

CT Intervention Design Considerations

During the design phase of that CT intervention, the main focus was placed on ensuring an effective entry of the CT into L-0 or L-1. Identification of each lateral was paramount to deliver the right treatment in the right lateral. As previously explained, lateral access

confirmation was obtained thanks to the real-time readings of the gamma ray. Pumping of the stimulation treatment was adjusted depending on the maximum depth reached by the CT through the use of the HPJN and the lateral identification tool activation process.

Selection of BHA for CT Downhole Parameters

A CT enabled with real-time telemetry provides bottom-hole readings of several parameters, such as pressure, temperature, casing collar locator, gamma ray, force (axial), and torque.

The first generation of the standard 2⅛" outside diameter (OD) downhole tools equipped with those sensors is shown in Table 1[5]. They were introduced for the stimulating of multilateral wells several years ago.

Since the aforementioned tools were limited to a pump rate of 2 barrels per minute (bpm), the stimulation process sometimes faced some limitations, such as longer pump durations, limited stimulation fluids penetration, or even the breakage of the fiber optics line because of its limited strength when highly viscous fluids were pumped.

Table 1 *Standard CT fiber optic telemetry and downhole measurements package[5].*

Standard System Sensors Package	
Maximum Flow Rate	2.0 bpm
Outside Diameter	2⅛"
Ball Drop	⅝"
Pressure Rating	12,500 psi
Operating Temperature	300 °F
Measurements	BHP, BHT, GR, DTS, CCL, TC
Fiber Optic	
Outside Diameter	0.071"

To address those limitations, a new high rate enhanced tool with 3¼" OD was specifically designed for multilateral wells stimulation. The comparison with the standard tool is shown in Table 2[5].

Thanks to its higher rate capabilities, the pumping duration was reduced by half; fluids can now penetrate deeper and at a higher velocity, thereby resulting in more efficient wormholes; finally, it's the joint introduction of a more resistant fiber optics line allowing the pumping of highly viscous fluids at higher pumping rates. The same gamma ray module was kept in the BHA so that access to the different laterals can be confirmed by comparing acquired gamma ray readings with reference gamma ray logs — obtained during well drilling.

It is important to highlight the importance of pressure gauges — one provides pressure inside the BHA and another outside, in the annulus. Pressure readings are indeed required to ensure that the fluid is injected at matrix acidizing rates, not exceeding the fracturing pressure. They are also leveraged to make sure the tools are functioning at their optimum operating pressures, e.g., usage of the lateral identification tool has been shown to be more effective when downhole pressure gauge readings are present rather than relying on surface pressure data acquisition.

HPJN to Increase Stimulation Fluids Penetration

Fluids exit the CT through an opening at the end of the BHA. For conventional stimulation operations, one can use a simple jetting nozzle, Fig. 2. A 360° high power rotating jetting nozzle, Fig. 3, or a HPJN, Fig. 4 and Fig. 5, can be used to enhance stimulation effectiveness by energizing the fluid as it exits the BHA.

The simple jetting nozzle does not rotate and features openings at different locations. When using it, the fluid does not impact the wellbore with the same force as that obtained when using either a 360° high power rotating jetting nozzle, or a HPJN. This means that higher pumping rates are required to reach the proper jetting effect and obtain an effective stimulation.

The 360° high power rotating jetting nozzle provides

Table 2 *Comparison between the standard and the enhanced fiber optic telemetry and downhole measurements package[5].*

	Standard System Sensors Package	**New Enhanced System Sensors Package**
Maximum Flow Rate	2.0 bpm	8.0 bpm
Outside Diameter	2⅛"	3¼"
Ball Drop	⅝"	1"
Pressure Rating	12,500 psi	12,500 psi
Operating Temperature	300 °F	325 °F
Measurements	BHP, BHT, GR, DTS, CCL, TC	BHP, BHT, GR, DTS
	Fiber Optic	**Fiber Optic**
Outside Diameter	0.071"	0.094"

longer coherent throw, using a lower pumping rate but with a higher power to obtain optimal clean out results. The jet impacts the wellbore at a 90° angle with a controlled rotation per minute (rpm), ensuring full contact with the wellbore. The 360° high power rotating jetting nozzle consists of a swivel that is powered by offset nozzles, which are available in numerous sizes in the head, Fig. 6. The size of the drift ring, head, and nozzle are all selectable and can be changed based on job requirements. The drift ring controls the size of the cuttings in cases when the 360° high power rotating jetting nozzle is used for clean out or helps in determining the well drifting conditions during the drift run.

Although it is highly desirable to use the 360° high power rotating jetting nozzle during stimulation treatments to take advantage of its well circumference coverage feature, one drawback is that it starts rotating as soon as pumping starts. It therefore makes it challenging to use such a nozzle during a CT intervention in a multilateral well, when it must be connected just below the lateral

Fig. 2 *A simple jetting nozzle.*

Fig. 3 *A 360° high power rotating jetting nozzle.*

Fig. 4 *The HPJN with orifices at different angles.*

Fig. 5 *The HPJN with orifices on the same plane.*

Fig. 6 *A diagram of a 360° high power rotating jetting nozzle.*

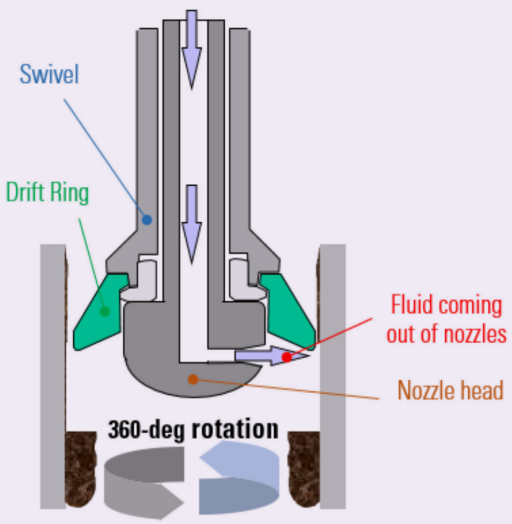

identification tool. The main challenge has to do with the pumping rate: first, the lateral identification tool only allows pumping up to a certain rate, which is not enough to properly operate the 360° high power rotating jetting nozzle. Then, the pumping rates at which the 360° high power rotating jetting nozzle rotates are likely to be the same as those for the activation of the lateral identification tool.

In recent years, the 360° high power rotating jetting nozzle has been successfully deployed below the lateral identification tool with the use of a valve that allows directing the flow toward either the 360° high power rotating jetting nozzle or the lateral identification tool, thanks to a specific opening and closing mechanism. It is, however, not an appropriate solution for wells like the candidate well because of the smaller 360° high power rotating jetting nozzle size relative to the bigger open hole, thereby leading to a lesser jetting impact on the rock face.

Considering the aforementioned limitations, the HPJN with orifices placed at different angles offered a better alternative. The main benefits of this solution are the following:

- The HPJN is available in bigger sizes compared to the 360° high power rotating jetting nozzle, and provides a better jetting effect relative to the wellbore diameter in the candidate well case.
- Its orifices come in numerous sizes; they can be placed at different angles or in the same plane, thereby providing the same benefit as the 360° high power rotating jetting nozzle to cover the entire wellbore circumference.
- It can be used above the lateral identification tool and activated through a simple ball drop mechanism once the latter has finished profiling the junction window, and the lateral has been accessed.
- It does not require a special valve to control the flow, as mentioned earlier for the 360° high power rotating jetting nozzle.

Lateral Identification Tool for Multilateral Access via CT

When a CT is RIH in a multilateral well, it normally follows the natural path, which, most of the time, corresponds to either the motherbore or the very last lateral that was drilled or completed. To access other laterals, a lateral identification tool is required. That tool is activated hydraulically. It is rigged up as the last section of the CT BHA. It features two major elements, which are the orienting tool and the controllable bent sub, Fig. 7.

The tool turns by 15° thanks to the orienting tool when pumping starts, and the rate goes over 1 bpm, with a steady pressure. The reader will note that the controllable bent sub presents a specific pumping/profiling rate with 500-psi to 800-psi pressure signal drop. As soon as pumping through the tool is stopped, the orienting tool turns another 15°. Therefore, for each pumping cycle, the tool turns a total of 30°, which results in 12 pumping cycles necessary to turn the tool by 360°. Each time the tool needs to be activated, up hole passes across the lateral window are conducted 12 times to record the unique pressure drop[6], Fig. 8.

To operate the lateral identification tool, the software not only displays tool orientation with respect to the lateral window, but it also shows the lateral identification tool profiling and/or mapping of the window. Each time the lateral window is mapped, the software memorizes the window orientation and monitors the BHA orientation throughout the entire mapping operation[7], Fig. 8.

Fig. 7 *The orienting tool in blue and controllable bent sub in orange.*

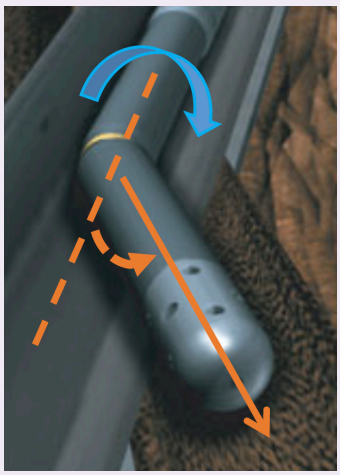

Fig. 8 *The lateral identification tool operation sequence: (1) Running across the junction, (2) Indexing, (3) Finding the lateral, and (4) Accessing the lateral.*

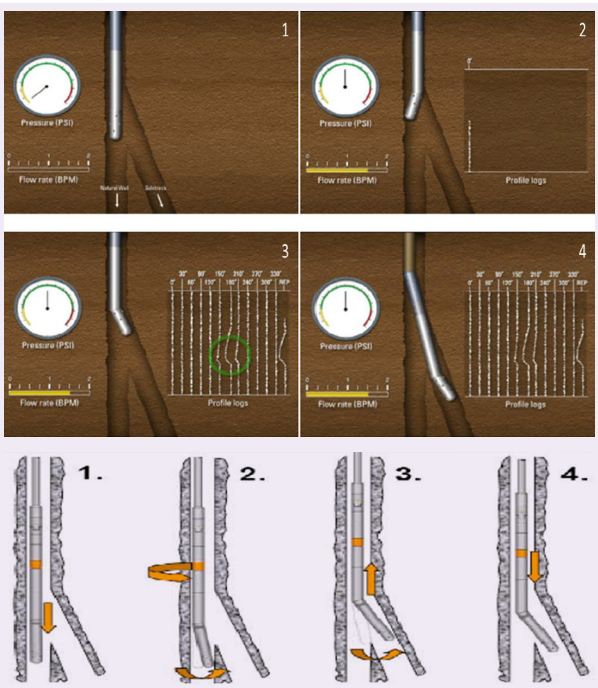

Figure 9 shows the final BHA after connecting all the aforementioned modules.

Job Execution Workflow and Procedures

An intensive collaboration between the operator and the service company resulted in defining the workflow and job procedures, Figs. 10a and 10b. The workflow and job procedures were established to leverage the results of real-time data acquisition during the actual intervention.

The main steps of that operation are presented as:

1. Lateral identification:
   - A gamma ray log was recorded while the CT was RIH, and each time the CT was entering either of the two laterals.
   - Each gamma ray log was correlated with the reference gamma ray log, which was recorded during the well drilling phase. This allowed the confirmation of which lateral the CT had entered.
2. Mapping/profiling each lateral using the lateral identification tool:
   - The lateral identification tool was placed 50 ft to 100 ft below the lateral window depth and water was pumped to activate the tool. Pumping continued until the orienting tool and controllable bent sub were fully activated. The CT was then pulled out of the hole (POOH) up to 50 ft to 100 ft above the lateral window depth.
   - After that up pass, pumping was stopped. The CT was RIH and the lateral identification tool positioned 50 ft to 100 ft below the lateral window depth. Step 1 was repeated. The process continued until 12 cycles were completed and the lateral mapping/profiling completed.
   - After pressure signals were analyzed and the best pressure response was identified for the respective orientations of the orienting tool and controllable bent sub, the lateral identification tool was activated again to orientate the tool in the desired direction. The CT was RIH to access the lateral, where the gamma ray was utilized as previously mentioned. Once the CT reached the open hole section, preflush was pumped.
3. HPJN Activation:
   - Once the maximum CT depth was reached, a ball was dropped to isolate the lateral identification tool and to activate the HPJN. The stimulation treatment was pumped while the CT was POOH.
   - The stimulation treatment consisted of several stages of 20% hydrochloric (HCl) acid and 20% viscoelastic diverting acid. After pumping the stimulation fluids, the CT was RIH while pumping the post-flush. Eventually, the CT was POOH while conducting the CT displacement.

Fig. 9 *The final BHA design used during the actual CT intervention.*

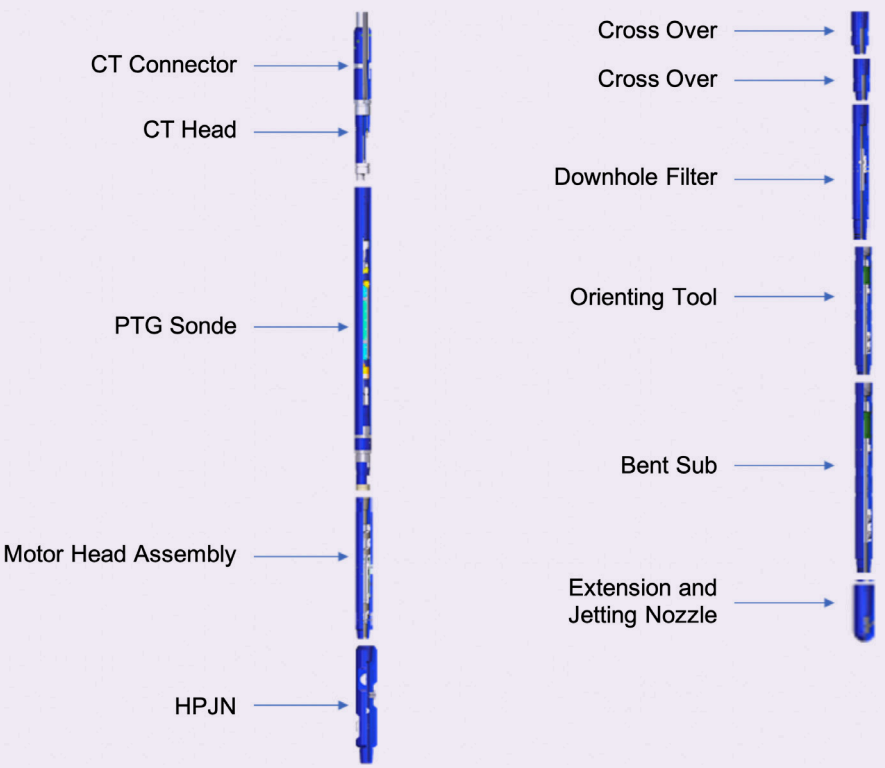

Fig. 10a *The established workflow for dual lateral well stimulation.*

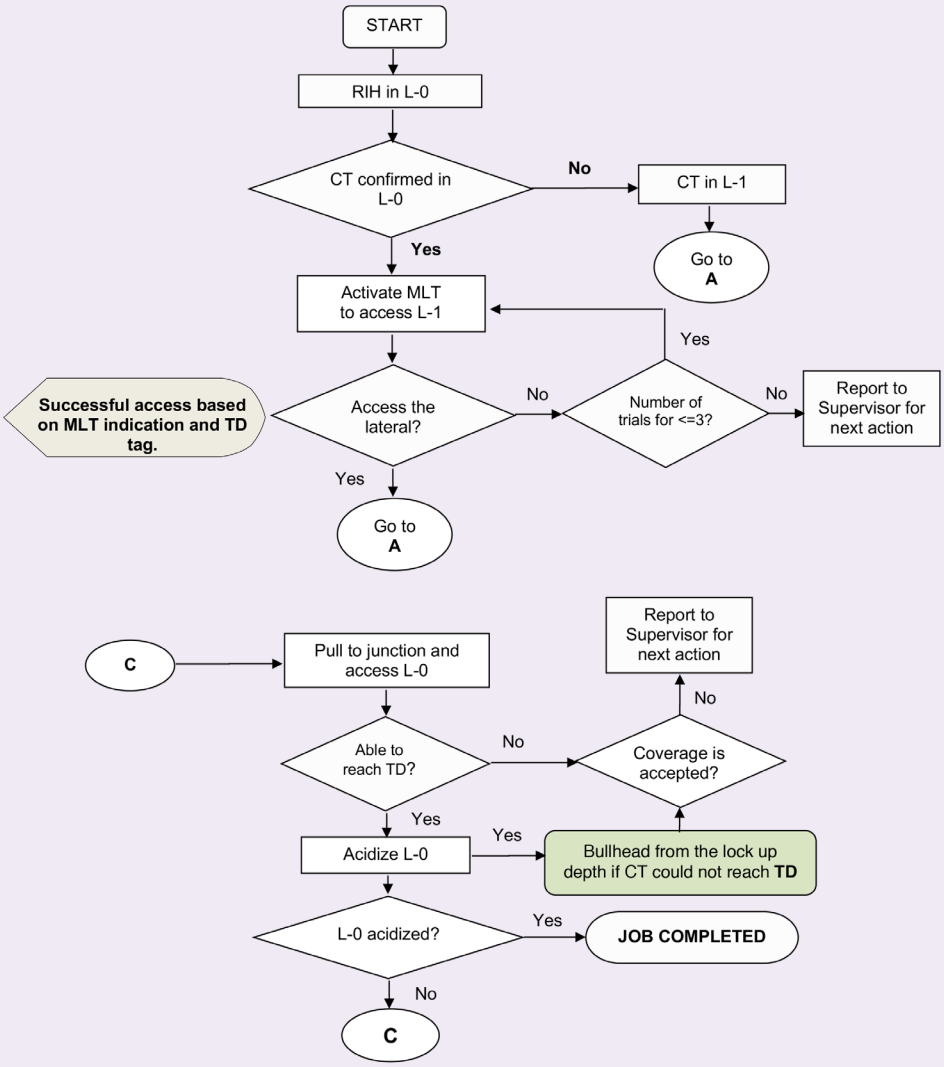

Job Execution

The operation was executed as per the designed workflow and job procedures. The intervention steps were updated based on the actual operational conditions, on a needed basis, and depending on the real-time downhole data acquisition.

As an example, even though the CT intervention was designed to be executed in a single run, the operation was eventually conducted in two runs, due to the battery life limitation of the downhole tools.

CT Run 1#

The CT surface and bottom-hole parameters for run #1 are shown in Fig. 11. The CT was RIH with the real-time downhole data acquisition tools, the HPJN, and the lateral identification tool. After establishing the circulation and obtaining clean returns at the surface, the CT entered the natural path, i.e., L-0. Entry in the motherbore was confirmed by correlating the acquired gamma ray with the reference log. The CT was run further in the hole while pumping water to the lockup depth that was deeper than the simulated CT reach depth.

The CT was then POOH until about 50 ft to 100 ft below the L-1 window. Mapping/profiling with the lateral identification tool was successfully conducted and the L-1 entered. As the CT entered the lateral, the ball was dropped to isolate the lateral identification tool and activate the HPJN. The CT was RIH, but it was stuck before being successfully freed. The RIH was continued while pumping the preflush. As soon as the CT reached the lockup depth, which was deeper than the simulated CT reach depth, the mixing of the stimulation fluids — 20% HCl acid and 20% viscoelastic diverting acid — started.

Once mixing was completed, the CT was POOH while delivering the stimulation fluids through the HPJN. Recurrent stages of 20% HCl acid followed by 20%

Fig. 10b *The established job procedures for dual lateral well stimulation.*

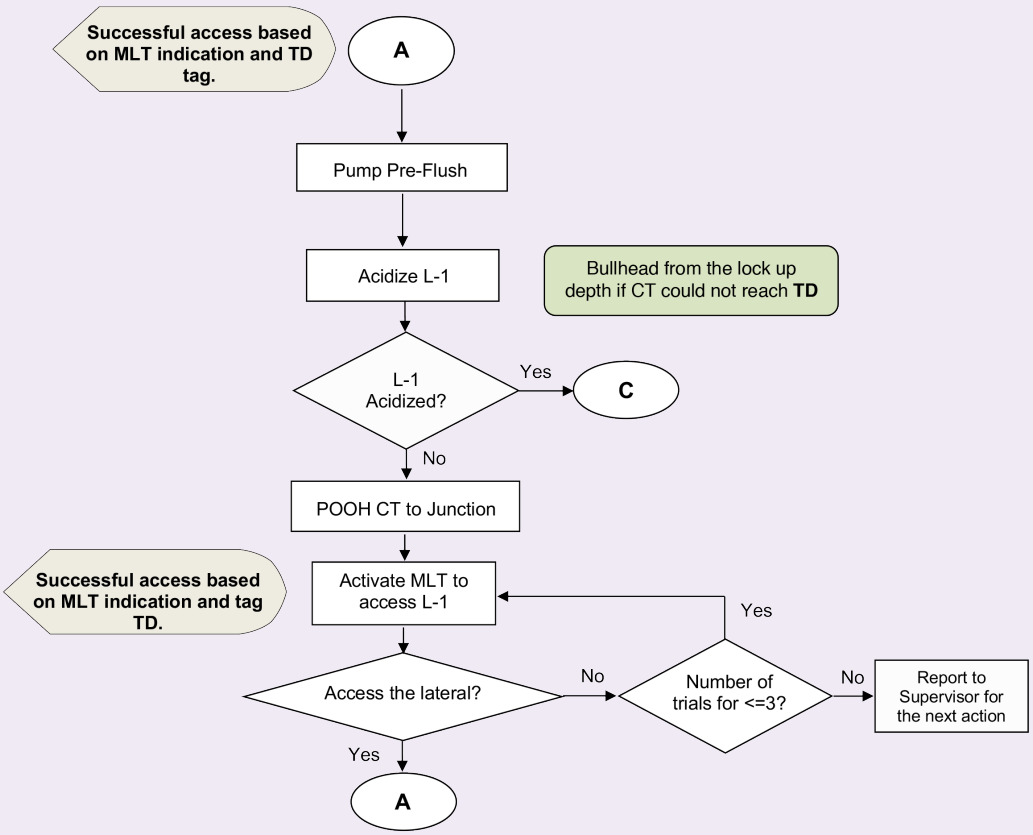

viscoelastic diverting acid were pumped following the job program during the stimulation. The CT had to be POOH to the surface to change the battery in the downhole tool for the next CT run, to stimulate L-0.

In addition, one of the lessons learned for similar treatments with regards to run #1 was that one had to conduct a complete wellbore displacement with treated water followed by a pre-stimulation injectivity test.

CT Run 2#

After changing the battery in the downhole tool, the CT was RIH for the second time with real-time downhole data acquisition tools, the HPJN, and the lateral identification tool. The CT surface and bottom-hole parameters during run #2 are shown in Fig. 12. The CT entered L-0 without the need for lateral identification tool activation, and gamma ray logging was used again to confirm the motherbore entry. The ball was dropped to isolate the lateral identification tool and activate the HPJN. The CT was RIH while pumping the preflush down to the lockup depth, which was the same as run #1.

Stimulation treatment was then initiated while following the same sequence as for run #1. Although, in both runs, the CT was able to reach deeper than the simulated CT reach, and it became evident during the operation that for future similar treatments, one should use bigger CT sizes in combination with CT reach enhancement tools. In addition, the pumping rates used during the stimulation treatment strictly followed the design. Based on the archived results, it was decided that for future operations, the pump rate would be brought up to 6 bpm to 8 bpm while keeping the pressure below the maximum wellhead and fracturing pressure limitation.

When the CT reached the surface, a post-stimulation injectivity test was performed using the available pumping capacity on location. The maximum injection rate was 7 bpm.

Lessons Learned

This intervention led to many lessons learned, which constitute the reference for similar operations in the future. They include:

- Conducting a pre-stimulation injectivity test and preferably conducting an injection/falloff test. It is because in the discussed well intervention, no injectivity test before stimulation treatment was conducted, and no comparison before and after the treatment was available.
- The utilization of a 2⅞" CT or its combination with tractors for deeper CT reach. The main reasons behind this idea is not only to obtain deeper CT

Fig. 11 *The CT surface and bottom-hole parameters during run #1.*

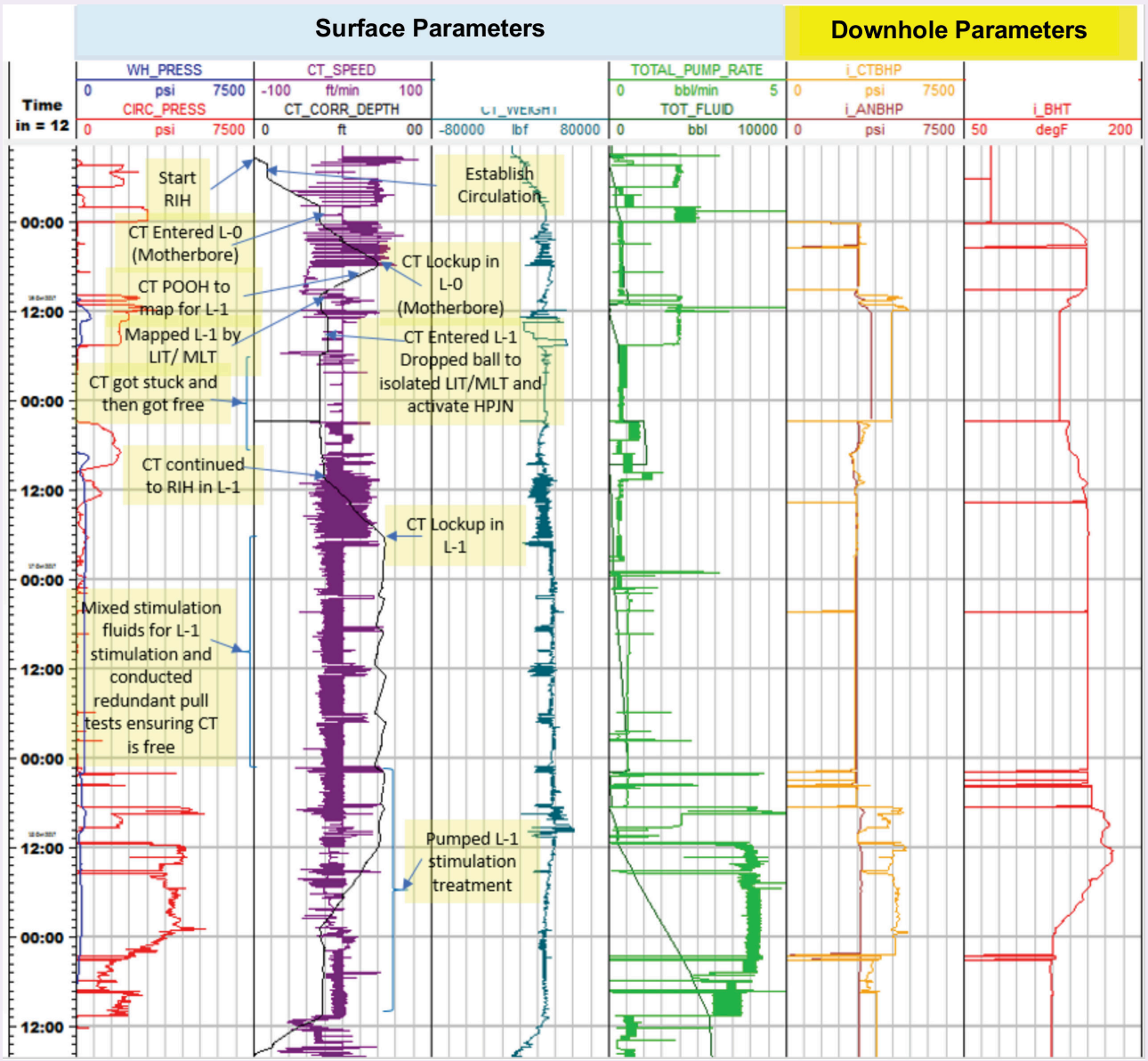

reach, but to also pump at higher rates for effective fluids and wormholes penetration, resulting in better damage removal.

- Reaching the maximum injection pressures of the high rate tool during stimulation treatment — 6 bpm to 8 bpm — while keeping the pressure below the maximum wellhead and fracturing pressure limitation.

Conclusions

The CT stimulation intervention in this field's first extended reach dual lateral power injector well was a success operationally, and met the job objectives.

The downhole readings were key in operating the lateral identification tool and mapping the lateral entry. They also helped optimize the delivery of the treatment by keeping the pumping of the stimulation treatment at the tools' optimal rate, below the fracturing pressure.

The entry in each lateral — L-0 and L-1 — was successfully confirmed using gamma ray logging. Finally, the HPJN enhanced the stimulation by providing a deeper penetration of the stimulation fluids.

Acknowledgments

The authors would like to thank the management of Saudi Aramco for their support and permission to publish this article.

This article was presented at the Abu Dhabi

Fig. 12 *The CT surface and bottom-hole parameters during run #2.*

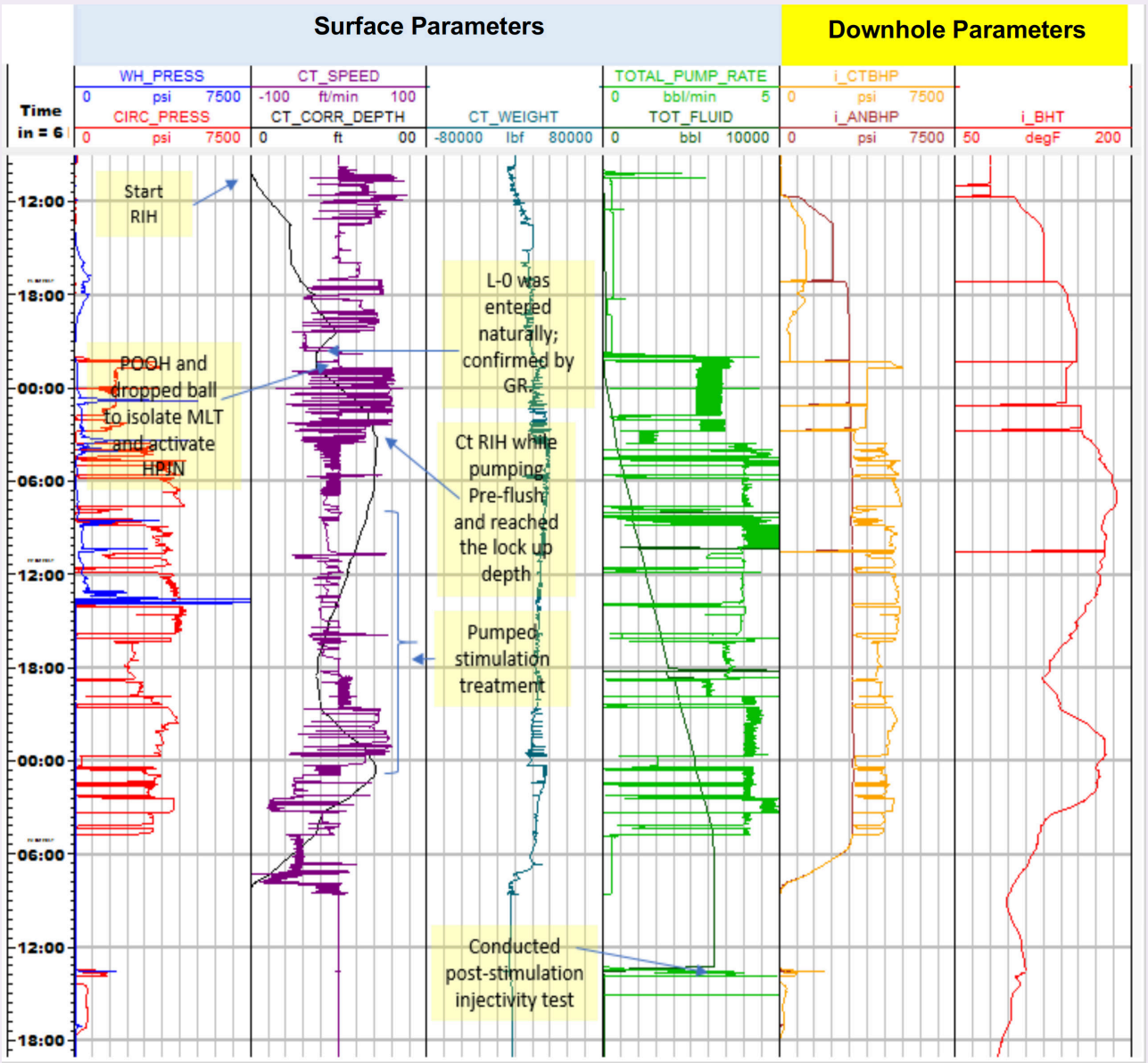

International Petroleum Exhibition and Conference (ADIPEC), Abu Dhabi, UAE, November 12-15, 2018.

References

1. Al-Gamber, S.D., Mehmood, S., Ahmed, D., Burov, A., et al.: "Tangible Values for Running Distributed Temperature Survey as Part of Stimulating Multilateral Injection Wells," SPE paper 167490, presented at the SPE Middle East Intelligent Energy Conference and Exhibition, Manama, Kingdom of Bahrain, October 28-30, 2013.

2. Cantaloube, F.Y.: "Optimization of Stimulation Treatments in Naturally Fractured Carbonate Formations through Effective Diversion and Real-Time Analysis," SPE paper 126136, presented at the SPE Intelligent Energy Conference and Exhibition, Utrecht, the Netherlands, March 23-25, 2010.

3. Garcia, S.J.R., Franco, E., Romandia, M.G., De Garate, E.D., et al.: "Revolutionary Matrix Stimulation Process in Offshore Mexico Using Coiled Tubing Equipped with Optical Fibers (CT-EOF) and Distributed Temperature Survey (DTS)," SPE paper 143318, presented at the SPE/ICoTA Coiled Tubing and Well Intervention Conference and Exhibition, The Woodlands, Texas, April 5-6, 2011.

4. Garzon, F.O., Amorocho, J.R., Al-Harbi, M., Al-Shammari, N.S., et al.: "Stimulating Khuff Gas Wells with Smart Fluid Placement," SPE paper 131917, presented at the SPE Deep Gas Conference and Exhibition, Manama, Kingdom of Bahrain, January 24-26, 2010.

5. Al-Buali, M.H., Abulhamayel, N., Leal, J., Ayub, M., et al.: "Recent Developments in Mechanical Descaling Operations: A Case Study from Saudi Arabia," SPE paper 173662, presented at the SPE/ICoTA Coiled Tubing and Well

Intervention Conference and Exhibition, The Woodlands, Texas, March 24-25, 2015.

6. Al-Jassem, H.M., Al-Shehri, A.M., Al-Shammari, N.S., Al-Gamber, S.D., et al.: "First Worldwide Coiled Tubing Stimulation of a Quadlateral Extended Reach Power Water Injector Using Multilateral Tool with Gamma Ray and Distributed Temperature Survey," SPE paper 183784, presented at the SPE Middle East Oil and Gas Show and Conference, Manama, Kingdom of Bahrain, March 6-9, 2017.
7. Al-Momin, A., Zeybak, M., Azrak, A.W. and Burov, A.: "First Successful Multilateral Well Logging in Saudi Aramco: Innovative Approach toward Logging an Open Hole Multilateral Oil Producer," SPE paper 149079, presented at the SPE/DGS Saudi Arabia Section Technical Symposium and Exhibition, al-Khobar, Saudi Arabia, March 15-18, 2011.

About the Authors

Hasan M. Al-Jassem

B.S. in Petroleum Engineering, University of Manchester

Hasan M. Al-Jassem is a Production Engineer with Saudi Aramco's Southern Area Production Engineering Department. He has 9 years of experience in production optimization, well intervention, well integrity management and intelligent fields. As part of Hasan's development assignments, he has worked as a Field Engineer, Plant Engineer and Well Site Foreman.

Hasan received his B.S. degree in Petroleum Engineering from the University of Manchester, Manchester, U.K.

Naji K. Al-Salman

B.S. in Chemical Engineering, King Fahd University of Petroleum and Minerals

Naji K. Al-Salman has been with Saudi Aramco since 2005. He is a Petroleum Engineer in the Southern Area Production Engineering Department (SAPED). Before joining Saudi Aramco, Naji worked as a Process Engineer at Bechtel for 4 years.

In 2001, he received his B.S. degree in Chemical Engineering from King Fahd University of Petroleum and Minerals (KFUPM), Dhahran, Saudi Arabia.

Rifat Said

B.S. in Mechanical Engineering, University of Indonesia

Rifat Said has more than 20 years of experience in the oil and gas industry, specifically in cementing, coiled tubing operations and stimulation services, including matrix stimulation and fracturing. He worked for Schlumberger for 18 years before joining Saudi Aramco in September 2006. Currently, Rifat works as a Stimulation Engineer providing technical support to the Southern Area Production Engineering Department.

In 1986, he received his B.S. degree in Mechanical Engineering from the University of Indonesia, Jakarta, Indonesia.

Danish Ahmed

M.S. in Petroleum Engineering, Heriot-Watt Institute of Petroleum Engineering

Danish Ahmed has been working at Saudi Arabia Schlumberger since 2007. He is the technical expert currently working with Schlumberger Well Services – Coiled Tubing Services. Danish's experience involves working as a Field Engineer with Well Production Services (Fracturing and Pumping Services) based in 'Udhailiyah, where he designed, executed and evaluated the proppant/acid fracturing and matrix acidizing jobs. Danish also worked as a Production Technologist with Petro-Technical Services (formerly called Data and Consulting Services) in Dhahran, Saudi Arabia.

In 2007, he received his M.S. degree in Petroleum Engineering from the Heriot-Watt Institute of Petroleum Engineering, Edinburgh, Scotland, U.K.

Kaisar Al Hamwi

B.S.E. in Telecommunication Engineering, University of Damascus

Kaisar Al Hamwi is a Technical Engineer, working for Schlumberger in Saudi Arabia. He has more than 12 years of experience in design, execution and evaluation of coiled tubing (CT) workover interventions in onshore environments with the highest service quality standards.

Kaisar's work supports Saudi Aramco in the technical aspects of CT interventions in oil, and power water injector wells, for matrix stimulation, descaling, perforating, clean outs, milling, fishing, zonal isolation, etc. Prior to this assignment, he was Field Service Manager for the 'Udhailiyah district, where he was responsible for service delivery and introduction of new technologies for CT and matrix stimulation.

Kaisar started his career in Syria as a Field Engineer for Schlumberger Well Services, and completed his field assignment in Saudi Arabia.

He has coauthored several Society of Petroleum Engineers (SPE) papers.

In 2007, Kaisar received his B.S.E. degree in Telecommunication Engineering from the University of Damascus, Damascus, Syria.

Effective Corrosion Mitigation Exploiting Glass Reinforced Epoxy Lined Tubulars in Offshore Producing and Injection Wells

Laurie S. Duthie, Hamad M. Almarri, Hussain A. Saiood, Ashwani K. Lata, and Gokul Radhakrishnan

Abstract /

Corrosion in offshore well completions can lead to serious well integrity problems and costly workover operations. Although carbon steel is an ideal material for most completions, under certain conditions, corrosion can attack and severely damage carbon steel equipment. Corrosion resistant alloys (CRAs) are a good option, but come with the considerable downside of very high cost. A relatively simple and cost-effective approach to protect completion equipment against these corrosive elements is to line carbon steel completion tubulars with a nonmetallic glass reinforced epoxy (GRE). The GRE material properties provide excellent protection against a range of conditions, including highly corrosive fluids, erosive granular materials, hydrogen sulfide (H_2S), carbon dioxide (CO_2), and acid treatments.

The GRE lined carbon steel is capable of combatting a range of corrosive environments in oil producers, water injector wells and supply wells, including water with a high concentration of total dissolved solids (TDS), chloride and sulfates, and oil with high levels of H_2S and CO_2. The steel tubing is protected from these unforgiving ecosystems by lining the inside of the tubing with one continuous GRE tube. To secure the GRE lining and to increase the strength, cement is pumped down the narrow annulus between the GRE lining and the tubing's internal wall. This procedure is relatively simple with the resultant GRE lined tubing having exactly the same tubing strength properties as the bare tubing.

The primary method for detecting any well integrity problems with water injector wells are from determining high pressures in the tubing casing annulus. To date, all of the water injector wells installed with 7" GRE lined tubing have remained integral with no indication of any corrosion. Several of the oil producer and water supply wells that were lined with GRE have subsequently been worked over to replace faulty equipment; primarily electric submersible pumps (ESPs). Encouragingly, the condition of the recovered GRE tubing had suffered no corrosion, scaling or other degradation benefiting from the GRE protection.

The nonmetallic GRE material is exceptionally robust with notable longevity, and is very resistant to any scale buildups, leading to improved flow assurance. At the same time, being tough enough to withstand any routine well intervention for logging, acid stimulation, and other applications. The durable qualities and chemical characteristics of these nonmetallic materials in downhole completions is likely to expand in the coming years, with increasing applications being found.

Background

Corrosion in well completions for offshore locations is a costly event to manage and repair; the level of complexity dealing with offshore logistics further add to the problem. One highly effective method to combat this corrosion is to install a nonmetallic glass reinforced epoxy (GRE) lining into the carbon steel pipe. The technology for lining tubing with GRE to provide a protective layer for carbon steel pipe has been around for many decades with over 100,000 installations worldwide[1]. The unique properties of the GRE lining makes it a relatively inexpensive option to combat against a range of hostile downhole conditions.

The versatile GRE lining is ideally suited for high hydrogen sulfide (H_2S) and carbon dioxide (CO_2) oil producers, highly corrosive water injector and water supply wells. This technology provides a viable alternative to the more expensive corrosion resistant alloys (CRA) and/or chemical inhibition treatments. The historic performance worldwide of GRE lining points to extremely long life, even in the harshest of environments.

GRE lining has been installed extensively in raw seawater injector wells since the early 1970s in the North Sea, with some still reported as being operational. The GRE lining not only extended the life of these water injector wells by many years, it also saved these operators large amounts of capital expense and associated operational expense to chemically treat the water[2].

Introduction

During a field development, lab studies are normally undertaken to understand the corrosive effects of the oil and water on the downhole carbon steel completions. To simulate downhole conditions, oil with high H_2S/CO_2

content and water with high total dissolved solids (TDS)/chlorides are experimented with at reservoir pressure and temperature. The data collected is modeled under different conditions taking into account the complex chemistry of crude oils, the viscosity, interfacial tension, density, flow regimes, flow parameters, water cut and other variables.

The results then show corrosion rates that could be expected under a range of conditions. The rate of corrosion is calculated using the weight loss method. This simply measures the amount of metal loss over a given time while the metal is immersed in the fluid. The rate of corrosion, R, mm per year is calculated as:

$$R = \frac{kW}{\rho A t} \quad (1)$$

where k = constant, W = total weight lost, t = time taken for the loss of metal, A = surface area of the metal, and ρ = density of the metal.

The results from these studies assist in the design and material selection of downhole equipment. Although undertaking these types of studies is good practice, the complex nature and various forms of corrosion, together with an evolving downhole environment over time make this a difficult area to predict and completely prevent; therefore, a single approach may not be possible. During the life cycle of a field, the approach may change in terms of corrosion prevention based on experience, and adapting to a changing environment.

Well Types

Three typical well category types were looked at: (1) oil producer, (2) water injector, and (3) water supply wells. As part of an overall corrosion strategy, a GRE liner is installed in the most vulnerable parts of oil producing wells, and the entire 7" tubing strings for water injector and water supply wells. For oil producer wells with electric submersible pumps (ESPs) installed and deep-set packers to protect the casing, 3 years is the average industry life expectancy in high H_2S/CO_2 environments.

Since the ESPs generally require replacement every 3 years, this allows for regular replacement of the 4½" L-80 tubing, and no serious corrosion is expected during this interval. The upper ESP tubing string stabs into a lower production string, which is normally not removed during regular ESP change out operations. This lower string is therefore exposed to the corrosive environment for much longer periods and requires a higher level of protection with a GRE liner installed in this tailpipe section.

A typical power water injector well is completed with a 7" monobore completion, and a GRE lined tubing string into the top of the liner with 6⅛" open hole injection sections. Water supply wells are regularly completed with 7" GRE lined tubing, including an ESP pump to boost the pressure and deliver higher rates.

Monitoring Techniques for Downhole Corrosion

1. Annuli Surveys: Quarterly surveys of the tubing casing annulus and casing-casing annulus pressures can reveal any communication caused by corrosion of the pipe. Although this is one of the easiest ways to monitor for corrosion, and is important to confirm well integrity, it is less than an ideal method since it will only become evident after the corrosion has done its damage. Subsequently, in combination with some of the other methods listed below, this can be part of an overall strategy.
2. Temperature Surveys: Deviation from the natural temperature gradient could be an indication of a corroded pipe with fluid flow behind the pipe.
3. Corrosion Logs: Time-lapse can be used to check for pipe variations over certain time intervals, and to identify any pitting or severe metal loss.
   - Mechanical: Multifinger caliper logs identify in high resolution any scale or corrosion present on the inner surface of any pipe logged, Fig. 1.
   - Acoustic: Ultrasonic logs measures the inner pipe scale and corrosion, along with any external metal loss, Fig. 2.
   - Electromagnetic logs: These logging tools can measure the total thickness of the pipes.

Fig. 1 *Multifingered caliper.*

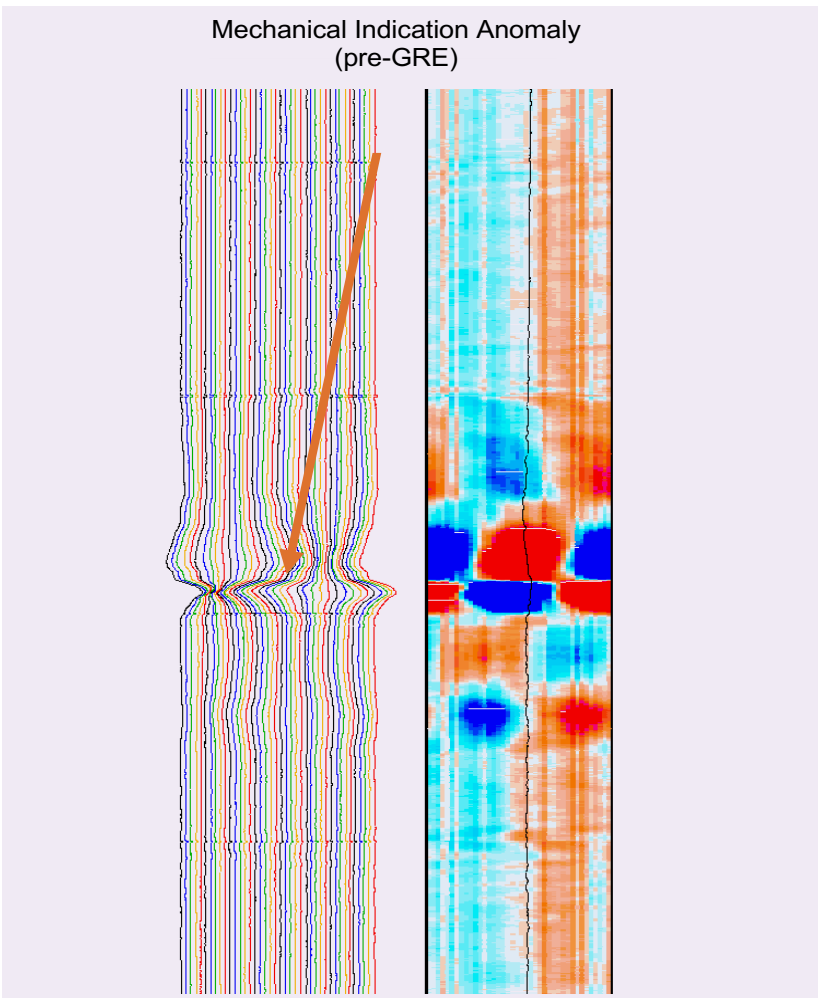

Fig. 2 *Ultrasonic log.*

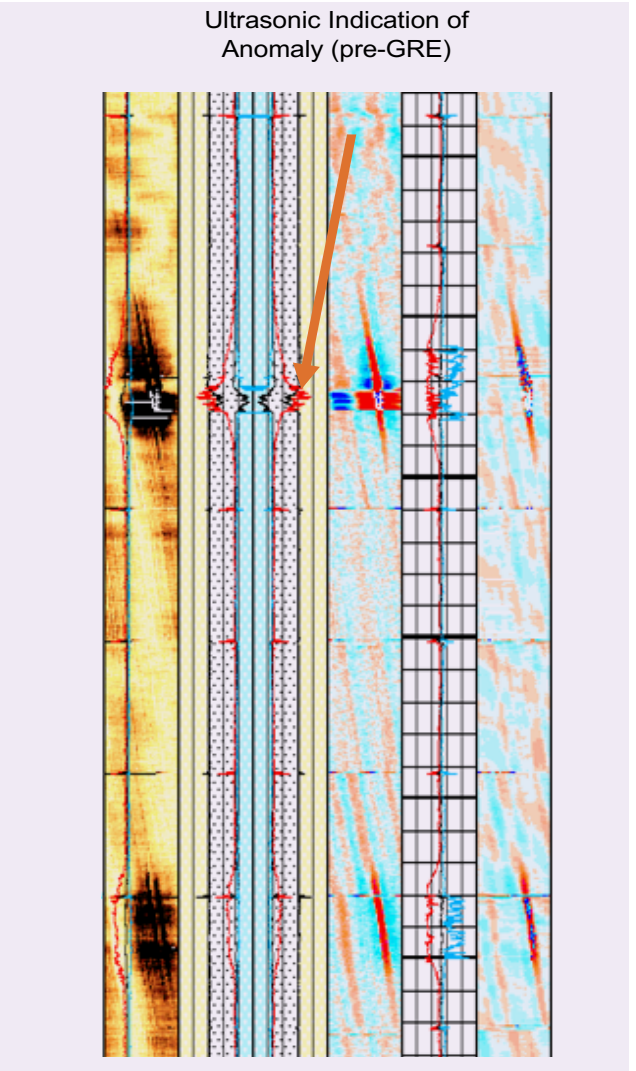

4. Corrosion Coupons: Using the same metal as the tubing/casing, coupons are placed in direct contact with the fluids and the rate of metal loss is measured over a certain period — usually several months.
5. Electrical Resistance Probes: Placed in the fluid at the surface, direct measurement of the metal loss of the electrical resistance probe allows a corrosion rate to be calculated. This can be monitored continually and be part of the data acquisition system to provide the metal loss rate, and allow for corrective measures to be taken if required.
6. Downhole Camera: A visual inspection of downhole tubing may reveal any corrosion in the pipe. This type of survey requires the tubing to contain clear fluid, or to be displaced to clear the fluid.
7. Visual Inspection: During workover operations, tubing is visually inspected for corrosion and other defects as it is pulled out of the hole; samples of the tubing may be analyzed for further investigation.

Corrosion Types and Causes

Oil and water contain all the main ingredients required for corrosion — high levels of H_2S and CO_2 in the oil and gas phases, high levels of chlorides, sulfates, and TDS in the water phases. Despite this, corrosion in the downhole completions can be kept at a sustainable level with a combination of extensive monitoring and implementation of corrective measures when any corrosion attacks are detected. Some of the common corrosion types that can occur in offshore wells and can also be very aggressive, are galvanic corrosion of dissimilar metallurgy, causing localized pitting mainly due to the elevated levels of TDS/sulfates/chlorides, and microbiological induced corrosion.

Corrosion Control Strategies

Starting with the most obvious solution, the best strategy is to avoid any downhole corrosion in the first place. This can be done by using 100% noncorroding materials in the well completions. Materials that can normally survive harsh downhole corrosive conditions are CRAs such as Super Duplex stainless steel and Incoloy 825, however, these are generally very expensive and not always the most practical solution.

Numerous methods of corrosion control exist for carbon steel pipe. The most economical and practical solution is to tailor these methods to match the well conditions that exist and to modify over time as they change. Cathodic protection is a common technique used to protect the external surface of the casing by electrically preventing the oxidation of the surface. Additional methods would include removing the corrosive elements from the fluids/gases, using chemical inhibition or having a chemical or physical barrier between the pipe and the corrosive fluid(s) and gases.

Chemical treatments include using corrosion inhibition chemicals, an oxygen scavenger to remove any free O_2 from the system, and injecting biocides to combat micro-bacterial activity. Corrosion inhibition may be introduced via surface injection in the case of water injection wells. For oil producers and water supply wells, the choices are downhole injection or intermittent squeeze jobs into the formation where the corrosion inhibitor is gradually released during normal flowing operations back up the well.

Internal Pipe Coating as a Corrosion Barrier

One option to provide a protective barrier to the internal part of any carbon steel pipe is to apply a coating such as an internal plastic coating (IPC). For this to be effective, the coating must be applied uniformly over the entire surface area of the pipe. One major disadvantage of IPC is that any defect during the application of the coating, such as a small area left uncovered, will leave the pipe vulnerable to a corrosion attack in that area.

Perhaps of even more of a concern is that even if the pipe achieves a perfect coating and provides a complete barrier to any form of corrosion, there will always exist a risk of damage during any well intervention. Avoiding any damage during intervention with downhole

tools on wireline or coiled tubing (CT) would require great attention to the types of tool ran and the actual deployment.

Using standard downhole tools during any well intervention creates a high probability that some damage will occur to the coating, and therefore, expose the bare metal to the corrosive environment. If the IPC becomes detached from the pipe, Fig. 3, it has the potential to plug a downhole ESP or other components in the well completion. For these reasons, IPC was not considered a viable alternative for this field application, although it should be noted that an external pipe coating is still a good solution to protect the outside of any pipe.

GRE Lining Decision

The internal GRE lining technology provides long lasting protection to downhole carbon steel tubing from corrosion due to process fluids/injection water. An inherently holiday free GRE composite liner is inserted inside a low cost carbon steel tubing and the annulus is filled with mortar, Fig. 4. The connection area is fully protected with the combination of flares and a corrosion barrier ring. The metal-to-metal seal in the premium connection is not affected by the lining system; in other words, the lining system does not interfere with the standard makeup of the premium connection.

The finished product has the combined high strengths of the steel with the corrosion resistance of GRE, to provide long lasting corrosion protection. The GRE lining was laboratory tested with various concentrations and combinations of H_2S and CO_2. Sweet tests were up to 10% CO_2 and 200 ppm H_2S while sour tests used concentrations of up to 10% CO_2 and 7% H_2S[3]. The resistance of the GRE lining to these elevated acid gas conditions supported the decision to use a GRE lining for the oil producer applications.

The GRE lining technology has been applied since 2002 in offshore oil producers[4], and the GRE installations were deployed in highly deviated wells. These wells were installed in 2002, and are still in operation, The connection with the GRE lining has been tested by the connection licensors up to 42° per 100 ft — above the usual deviation. The technology was approved after a successful 8-year pilot testing, including carrying out multifinger caliper logs through the production tubing to monitor the condition. The results were satisfactory, and the technology was accepted for implementation.

GRE Liner Additional Benefits

The smooth surface of the GRE lining brings a few additional benefits. The internal surface of the GRE is finished to a low 0.00021" level of smoothness — this compares to 0.00138" for carbon steel. This smoother surface impedes the build up of elements that could

Fig. 3 *ESP plugged by IPC.*

Fig. 4 *GRE lining process.*

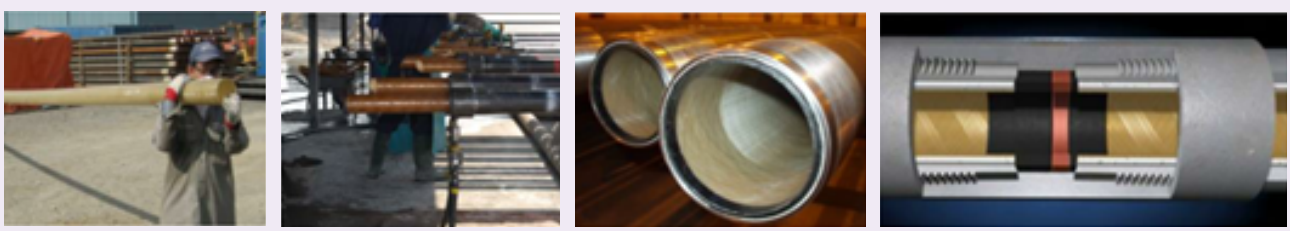

Table 1 *Tubing condition after inspection.*

Number of GRE lined joints inspected.	Number of joints with liners in good condition — can be reused after cleaning, standard flare replacement, connection repair, etc.	Number of joints rejected and the reason.
8 joints	7 joints	1 joint due to liner stinger near to the pin end.

adhere to the surface, such as asphaltenes or wax. The other benefit of the smoother surface is a reduction in friction with smaller pressure drops when compared to carbon steel[5]. The GRE liner is also suitable for relatively high downhole temperatures up to 280 °F, covering the majority of oil, gas, and water well completions.

Completion Consideration

GRE lined completions requires a minor redesign of the completion to accommodate the reduction in the inside diameter (ID) of the tubing. The impact of these had to be evaluated based on the flow rate impact and completion accessory resizing. Besides, operational issues relating to logging the well, and setting plugs in the well have to be considered[6].

In terms of flow rates and pressures, there has never been any recorded drop after installation of the GRE lined tubing. As an added benefit, in the absence of scaling and interruptions, the GRE lined completions can inject or produce relatively more fluids than the unlined carbon steel completions.

In the case of injection wells, downhole nipples are removed to make way for the reduced ID of the GRE lined completions. The initial carbon steel completion is equipped with an X/R nipple in the upper completion. Subsequently, in the interest of not having to reduce the ID to fit the nipple profile size to suit the GRE lined tubing completion, the X/R nipple can be eliminated.

For a GRE lined tubing completion, standard bridge plugs cannot be used since the sleeves would damage the GRE liner, however, there are other available alternative options:

1. Inflatable plug/packers can be used, as GRE lined tubing has been tested with inflatable plugs successfully.
2. Expandable bridge plugs can be used, which can pass through the GRE lined tubing, and can be set on an unlined cemented liner below.
3. Unlined CRA joints, suitable to handle oxygen corrosion, can be used where standard bridge plug intervention is planned in the future. Based on the National Association of Corrosion Engineers standards and industry experience, it is recommended to use 25 chrome (Cr) super duplex stainless steel unlined joints for water injector wells, to fully handle oxygenated water.

Performance Evaluation of GRE Lined Tubing

Various corrosion logs were reviewed for a GRE lined oil producer, water injection and water supply wells without showing any corrosion indication. Some completions with GRE lined carbon steel have been pulled to replace failed ESPs, with none of these wells suffering any appreciable corrosion.

Well-1, a water supply well, was pulled out after 4 years due to ESP failure. This provided an additional chance for inspection of the liner's behavior when exposed to water with high levels of TDS, sulfates, and chlorides. The inspection report shows the removed GRE lined tubing in overall good condition, Table 1.

Fig. 5 *GRE lined tubing that was pulled out from a water supply, Well-2.*

Table 2 *Tubing condition after inspection.*

Number of GRE lined joints inspected	Number of joints with liners in good condition — can be reused after cleaning, standard flare replacement, connection repair, etc.	Number of joints rejected and the reason.
8 joints	8 joints	None

Table 3 *Relative cost comparison between carbon steel tubing and Cr tubing.*

Type	Cost/Ft	Cost for Length of 5,500 ft
7" #26 L-80 carbon steel tubing with GRE lining	1	$5,500
7" #26 L-80 25 Cr alloy tubing	2.5	$13,750

Table 4 *The anticipated life span of three types of wells using GRE lined tubing.*

Type of Well	Expected Life Span
Oil Producer	3 years because of ESP
Water Injector	10 to 15 years
Water Supply	5 years because of ESP

Well Integrity Evaluation and Results

Figure 5 shows a GRE lined tubing that was removed and inspected.

Well-2, a water supply well, is GRE lined with 13 Cr tubing instead of carbon steel tubing to protect the OD from corrosion. This tubing was retrieved after ESP failure and after 2 years in the hole. The inspection report shows the removed GRE lined tubing in good condition, Table 2.

Oil Producer Wells

In the oil producer wells, even with elevated levels of H_2S or CO_2, no corrosion of any consequence was noted. The relatively frequent replacement of ESPs limits the exposure of bare L-80 steel to around 3 years; inspection of the retrieved tubing has shown only general low-level corrosion.

Lower completions are installed with a GRE liner from the outset with several of these lower completions retrieved to allow for reentry purposes. The inspection of the tailpipe section after periods of up to 10 years in the hole showed the GRE and pipe in excellent condition with no scale build up, where the degradation of the GRE material or corrosion provided an effective internal barrier to the tubing.

Workover Economics/Cost Avoidance

Table 3 illustrates the international current relative cost per ft of 7" #26 L-80 carbon steel tubing with a GRE lining and for 7" #26 L-80 25 Cr tubing. The 25 Cr alloy tubing has a 250% cost premium to the equivalent GRE lined tubing, demonstrating the significant cost savings that can be made by selecting the GRE lined tubing.

Table 5 *Relative capital and operational costs.*

	Carbon Steel	GRE Lined Carbon Steel
Capital cost	1	2.62
Workover cost	1	1
Total cost per workover	1	1.26
Estimated workovers in 15 years	3	0
Projected cost in 15 years	2.4	1

Table 4 shows the anticipated life span of the tubing in three different types of wells using the GRE lined tubing.

Consequences of Corrosion

1. Interruption to oil production and water injection/supply.
2. Delays waiting for workover rigs to be moved to the location.
3. Expensive workover costs for onshore water injection wells, and by an additional magnitude for offshore wells.

Table 5 lists the relative values/ratios used in the tabulation of project costs and benefits.

Typically, the extra capital investment made on GRE lined completion is normally found to be recovered before the first workover of a standard carbon steel completion.

Conclusions

Clearly, having an effective barrier between the carbon steel tubing and the corrosive fluids is one of the easiest and lowest cost methods to protect a valuable asset. The additional capital outlay at the outset is comparatively marginal against the total well cost and can bring major cost savings.

The benefits of GRE lined tubing have been clearly demonstrated in a range of well types from oil producers to water injection and water supply wells. The major benefits include:

- Corrosion resistance in high concentrations of H_2S, CO_2, TDS, sulfates, and chloride.
- Highly resistant to most chemical treatments, including up to a 20% concentration of hydrochloric acid.
- Low cost in comparison to CRA, providing a similar level of corrosion resistance.
- Very durable material allowing well intervention with most conventional tools using a wireline or CT.
- Reduced interruption to production/injection with increased well life.
- Reduced overall cost for the well life span, with exaggerated cost savings for offshore installations.
- Improved flow assurance, no scale build up, proven longevity.

Although the technology has been around for decades, in more recent years, there has been an increased realization of the benefits of nonmetallic materials with serious research and development ongoing into these products. Currently, there are 100% nonmetallic high strength composite tubulars already existing in the market, these high strength composite tubulars are much lighter than steel, although only suitable for lower pressures compared to steel and GRE lined steel completions. With continued improvements in the engineering of nonmetallics, one could expect high performance nonmetallic solutions to become more widely exploited in the coming years.

Acknowledgments

The authors would like to thank the management of Saudi Aramco and Maxtube for their support and permission to publish this article.

This article was presented at the Offshore Technology Conference, Houston, Texas, May 6-9, 2019.

References

1. Radhakrishnan, G., Kumar Sharma, A.L., Venkataraman, E. and Fernandes, A.: "Enhanced Life Cycle Costing Approach to Tubing Material Selection — New Cost and Revenue Drivers Identified from Experience with Nonmetallics Downhole," SPE paper 192775, presented at the Abu Dhabi International Petroleum Exhibition and Conference, Abu Dhabi, UAE, November 12-15, 2018.
2. Fernandes, A., Radhakrishnan, G. and Al Farisi, O.: "Regional and International References for the Implementation of GRE Lining Technology for Downhole Tubing to Improve Flow Assurance in Abu Dhabi Oil and Gas Upstream Applications," paper presented at the SEG/AAPG/EAGE/SPE Research and Development Petroleum Conference and Exhibition, Abu Dhabi, UAE, May 9-10, 2018.
3. Waterton, K., Savino, V., Radhakrishnan, G. and Simpson, J.: "Application of Glass Reinforced Epoxy (GRE) Lining Barriers in Downhole Tubing for Gas Production under Sour Conditions," paper 77-NM-08, presented at the 14th Middle East Corrosion Conference and Exhibition, Manama, Kingdom of Bahrain, February 12-15, 2012.
4. Sharif, Q.J., Esmail, O.J., Radhakrishnan, G., Simpson, J.A., et al.: "Experience with Fiberglass (GRE) Lined Carbon Steel Tubular for Corrosion Protection for Oil Production Applications," SPE paper 160236, presented at the SPE Annual Technical Conference and Exhibition, San Antonio, Texas, October 8-10, 2012.
5. Simpson, J.A. and Radhakrishnan, G.: "Developments and Experience in Nonmetallic Alternatives to Combat Corrosion in the Oil and Gas Business," paper prepared for presentation at the Effective Environment Management through Continual Corrosion Control Conference, Bidholi, Dehradun, India, November 25-26, 2006.
6. Radhakrishnan, G., Bremner M. and Simpson, J.A.: "Downhole Completion Considerations while Applying GRE Lining Barriers to Downhole Tubing for Corrosion Protection," paper 10126, presented at the 13th Middle East Corrosion Conference and Exhibition, Manama, Kingdom of Bahrain, February 14-17, 2010.

About the Authors

Laurie S. Duthie

M.S. in Petroleum Engineering
University of New South Wales

Laurie S. Duthie joined Saudi Aramco in 2011 as a Petroleum Engineer focused on the development and production of a large offshore field in the Northern Area. He started his career in 1986 on offshore installations in the U.K. North Sea as a Field Engineer in well testing and wireline operations. Laurie has a strong background in reservoir surveillance, well intervention, acid stimulation, well testing, completions, and cased hole logging. He has gained extensive operational experience in diverse remote onshore and offshore locations — across Africa, Central Asia, the former Soviet Union, Asia Pacific and in the Middle East region since 2009.

Laurie received his M.S. degree in Petroleum Engineering in 2005 from the University of New South Wales, Sydney, Australia.

Hamad M. Almarri

M.S. in Energy and Mineral Engineering,
Pennsylvania State University

Hamad M. Almarri is a Production Engineer in the Manifa Production Engineering Unit under the Northern Area Production Engineering and Well Services Department. From 2009 to 2013, Hamad spent one year with the Safaniyah Production Engineering Unit, one year with the Manifa Reservoir Management Unit and almost two years with the Manifa Production Engineering Unit.

In 2009, he received his B.S. degree in Petroleum Engineering from the University of Louisiana at Lafayette, LA, and began working with the Safaniyah Production Engineering Unit as a Production Engineer.

In 2015, Hamad received his M.S. degree in Energy and Mineral Engineering from Pennsylvania State University, State College, PA.

Hussain A. Al-Saiood

B.S. in Petroleum Engineering,
University of Oklahoma

Hussain A. Al-Saiood is a Production Engineer working in the Manifa Production Engineering Division of Saudi Aramco's Northern Area Production Engineering and Well Services Department. Joining Saudi Aramco as a Petroleum Engineer, he has also held several drilling and reservoir engineering positions, covering several onshore and offshore fields. Hussain's areas of interest include rigless intervention with coiled tubing (CT), wireline, and hydraulic workover operations.

Throughout his career, he has worked in multiple projects, including the change out of electric submersible pumps utilizing the hydraulic workover unit, and developing downhole equipment to enhance the CT reach, i.e., CT tractors and pulsation tools, in extended reach wells for stimulation and logging applications.

Hussain received his B.S. degree in Petroleum Engineering from the University of Oklahoma, Norman, OK.

Ashwani K. Lata

B.Eng. in Metallurgical Engineering,
Malaviya National Institute of Technology

Ashwani K. Lata is a Metallurgical Engineer by training with 21 years of work experience in various upstream domains, such as automated dewatering systems, surface facilities, multiphase flow metering, oil country tubular goods material selection, and nonmetallics. He works for MaxTube Limited as Sales Manager for Saudi Arabia and Bahrain — promoting his company's fiberglass (glass reinforced epoxy (GRE)) lining services for downhole tubing for corrosion protection.

Lata's expertise involves providing recommendations to his customers as to when to use nonmetallics based on technical suitability and commercial attractiveness, along with helping to modify completions to suit the GRE lining.

He is an active member of the Society of Petroleum Engineers (SPE).

Lata received his B.Eng. degree (with honors) in Metallurgical Engineering from Malaviya National Institute of Technology, Jaipur, Rajasthan, India.

Gokul Radhakrishnan

B.Eng. in Chemical Engineering,
Birla Institute of Technology and Science

Gokul Radhakrishnan is a Process Engineer by training with 30 years of work experience in various upstream domains, such as control systems, surface facilities, multiphase flow metering, Oil Country Tubular Goods (OCTG) material selection and nonmetallics. He works for MaxTube Limited as Regional Manager — Middle East and North Africa and Southeast Asia — promoting his company's fiberglass (GRE) lining services for downhole tubing for corrosion protection. Gokul's expertise involves making recommendations to his customers when to use nonmetallics based on technical suitability and commercial attractiveness, along with helping to modify completions to suit the GRE lining. He has been actively involved in the testing of the GRE liners for Saudi Aramco for sweet and sour gas production applications.

Gokul is an active member of the Society of Petroleum Engineers (SPE) and the National Association of Corrosion Engineers (NACE) and has coauthored several papers on multiphase metering and GRE lined completions for production and injection applications.

He received his B.Eng. degree (with honors) in Chemical Engineering from Birla Institute of Technology and Science, Pilani, Rajasthan, India, and his Post-Graduate Diploma in International Trade, from the Indian Institute of Foreign Trade, Mehruli, New Delhi, India.